frontiers | Frontiers in Chemistry

ORIGINAL RESEARCH
published: 05 July 2022
doi: 10.3389/fchem.2022.884050

Electrochemical Sensor for Hydrogen Peroxide Based on Prussian Blue Electrochemically Deposited at the TiO_2-ZrO_2–Doped Carbon Nanotube Glassy Carbon-Modified Electrode

Lenys Fernández[1], Jocelyne Alvarez-Paguay[1], Gema González[2,3], Rafael Uribe[4], Diego Bolaños-Mendez[1], José Luis Piñeiros[1], Luis Celi[5] and Patricio J. Espinoza-Montero[1]**

[1]Escuela De Ciencias Químicas, Pontificia Universidad Católica Del Ecuador, Quito, Ecuador, [2]Yachay Tech University, School of Physical Sciences and Nanotechnology, Urcuqui, Ecuador, [3]Instituto Venezolano De Investigaciones Científicas, Centro De Ingeniería Materiales y Nanotecnología, Caracas, Venezuela, [4]Departamento De Ingeniería Química, Escuela Politécnica Nacional, Quito, Ecuador, [5]Departamento De Física, Escuela Politécnica Nacional, Quito, Ecuador

OPEN ACCESS

Edited by:
Baiqing Yuan,
Ludong University, China

Reviewed by:
Lin Liu,
Anyang Normal University, China
Jingchao Zhang,
Anyang Normal University, China

***Correspondence:**
Lenys Fernández
lmfernandez@puce.edu.ec
Patricio J. Espinoza-Montero
pespinoza646@puce.edu.ec

Specialty section:
This article was submitted to Electrochemistry, a section of the journal Frontiers in Chemistry

Received: 25 February 2022
Accepted: 04 May 2022
Published: 05 July 2022

Citation:
Fernández L, Alvarez-Paguay J, González G, Uribe R, Bolaños-Mendez D, Piñeiros JL, Celi L and Espinoza-Montero PJ (2022) Electrochemical Sensor for Hydrogen Peroxide Based on Prussian Blue Electrochemically Deposited at the TiO_2-ZrO_2–Doped Carbon Nanotube Glassy Carbon-Modified Electrode. Front. Chem. 10:884050. doi: 10.3389/fchem.2022.884050

In this investigation, a hydrogen peroxide (H_2O_2) electrochemical sensor was evaluated. Prussian blue (PB) was electrodeposited at a glassy carbon (GC) electrode modified with titanium dioxide– and zirconia-doped functionalized carbon nanotubes (TiO_2.ZrO_2-fCNTs), obtaining the PB/TiO_2.ZrO_2-fCNTs/GC-modified electrode. The morphology and structure of the nanostructured material TiO_2.ZrO_2-fCNTs was characterized by transmission electron microscopy, the specific surface area was determined *via* Brunauer–Emmett–Teller, X-ray diffraction, thermogravimetric analysis, and Fourier transform infrared spectroscopy. The electrochemical properties were studied by cyclic voltammetry and chronoamperometry. Titania-zirconia nanoparticles (5.0 ± 2.0 nm) with an amorphous structure were directly synthesized on the fCNT walls, aged during periods of 20 days, obtaining a well-dispersed distribution with a high surface area. The results indicated that the TiO_2.ZrO_2-fCNT–nanostructured material exhibits good electrochemical properties and could be tunable by enhancing the modification conditions and method of synthesis. Covering of the nanotubes with TiO_2-ZrO_2 nanoparticles is one of the main factors that affected immobilization and sensitivity of the electrochemical biosensor. The electrode modified with TiO_2-ZrO_2 nanoparticles with the 20-day aging time was superior regarding its reversibility, electric communication, and high sensitivity and improves the immobilization of the PB at the electrode. The fabricated sensor was used in the detection of H_2O_2 in whey milk samples, presenting a linear relationship from 100 to 1,000 μmol L^{-1} between H_2O_2 concentration and the peak current, with a quantification limit (LQ) of 59.78 μmol L^{-1} and a detection limit (LD) of 17.93 μmol L^{-1}.

Keywords: carbon nanotubes, titania nanoparticles, zirconia nanoparticles, Prussian blue, electrochemical sensors

1 INTRODUCTION

A sensor is a device that allows the transformation of a physicochemical process into an analytical signal, through a recognition element that connects the analyte with the transducer, showing an electrical signal (Yan et al., 2015). The proper design of a sensor is of utmost importance so that the results of any analysis are accurate and at the same time reliable. Therefore, nanotechnology, electrochemistry, and analytical chemistry have been combined developing devices with diagnostic capacity (Srinivasan et al., 2015).

Electrochemical sensors take advantage of the redox characteristic of chemical species for the development and application of analytical techniques. Electrochemical techniques are very attractive because they do not generate a high cost, have a fast response, and are easy to integrate into complex investigations.

For an electrochemical sensor to have a good performance, the recognition element must be correctly immobilized on its surface, where the design and development of simple and compatible materials are extremely important. In order to reach the latter, organic (Li et al., 2016) and inorganic nanomaterials are properly combined to obtain the optimum efficiency. This is an emerging area in nanotechnology.

Carbon nanotubes (CNTs) have been the subject of much research due to their unique and remarkable mechanical, electrical, thermal, and elastic properties. CNTs have a relevant application in nanodevices, particularly in sensors, where they are used to increase analytical performance, when they are functionalized with suitable materials and through interconnection and transduction processes on their surface.

For a good performance of the CNT as part of an electrochemical sensor, its surface must be chemically modified (Montes et al., 2016). Metal oxide nanoparticles bound to CNT surfaces have received notable interest due to their applications in the design of functional nanostructures in electrochemistry that include high adsorption capacity, catalytic properties, biocompatibility, and suitable surface sizes that favor the efficient interaction of the analyte on the sensor (Solanki et al., 2011; Srinivasan et al., 2015; Montes et al., 2016).

Prussian blue (PB) is an inorganic compound widely used to modify electrodes for electrochemical sensors. The most important feature of PB when it comes to analytical applications is its electrocatalytic activity for the reduction of hydrogen peroxide (H_2O_2) and oxygen (Itaya et al., 1984). Electrodeposition of PB under certain conditions has been reported to lead to the synthesis of a selective electrocatalyst to reduce H_2O_2 in the presence of oxygen (Karyakin et al., 1996). Due to its high activity and selectivity, which are commonly the properties of biological catalysts, PB has been called artificial peroxidase (Itaya et al., 1984). PB as the H_2O_2 transducer is very advantageous (Karyakin et al., 2004) compared to the platinum electrode (the electrocatalyst part that has been regarded as the benchmark for H_2O_2 and O_2), and PB-modified electrodes are three orders of magnitude more active and selective in the reduction and oxidation of H_2O_2 in neutral media in the presence of oxygen (Karyakin et al., 1996).

The monitoring of low levels of H_2O_2 is of great importance for modern medicine, environmental control, and various branches of industry (Gutiérrez et al., 2011; Lv et al., 2020; Shu and Tang, 2020; Wang et al., 2020; Zhang et al., 2020; Hou et al., 2021; Xu et al., 2021). In particular, in biological applications, for example, there is the presence of H_2O_2 in the human body that is converted into OH radicals with high reactivity; an overproduction of OH and O_2 at cell openings promote cell damage and tissue malfunctioning (Rhee et al., 2010; Grisham, 2013). Similarly, the detection of H_2O_2 is a diagnostic response of medical devices such as glucose sensors, which are in the presence of oxygen, where H_2O_2 is produced by the action of glucose oxidase (Sajjadi Kouchesfehani et al., 2017). They also play an essential role in everyday life, such as monitoring food, bleaching processes, and even regulating human metabolic processes. Therefore, the detection of H_2O_2 is of relevant importance.

The combination of PB with CNTs and nanostructured metal oxides (Roushani et al., 2013a; Roushani et al., 2013b; Salimi et al., 2013; Roushani and Karami, 2014; Roushani and Dizajdizi, 2015; Roushani and Dizajdizi, 2016) can generate novel results for good electrical communication between the recognition system and the electrode surface. Zirconium oxide (ZrO_2) nanoparticles have been used as an electrochemical biosensor platform for oral cancer detection by cyclic voltammetry (Zong et al., 2007; Zhao et al., 2020; Rathee et al., 2021). A nanostructure material from ZrO_2 nanoparticles on CNTs was used to immobilize myoglobin showing excellent electrocatalytic activity for the reduction of H_2O_2 (Yang et al., 2020). On the other hand, titanium dioxide (TiO_2) has a large surface area and unique electronic and chemical properties (Zhang et al., 2011; Bai and Zhou, 2014; Liu et al., 2017; Guerrero et al., 2019). Considering its electronic band structure, TiO_2 is rich in electrons and belongs to the category of n-type semiconductors. TiO_2 nanomaterials are used for sensors in the detection of organic compounds that are soluble in aqueous media. Furthermore, they are used for the detection of gases and biological and chemical substances. Consequently, it may be stated that research on electrochemical sensors indicates that the immobilization of the recognition system is a task that must be fulfilled in order to produce an electrical connection between the analyte and the electrode. The modified CNTs facilitate the detection of a good interconnection path, and this would lead to a better detection of H_2O_2 that has an improved response in the analysis (Li et al., 20182018).

The development of catalysts for H_2O_2 reduction is of major interest for electrochemical sensors. PB is a cheap, efficient, and robust catalyst for H_2O_2 reduction, whose simple preparation allows the development of a series of H_2O_2 sensors on the nanometer scale with the advantage to miniaturize operational devices and promising to probe in real time the production of H_2O_2 in living cells by using nanoelectrodes. In this context, the present work presents the development of an electrochemical H_2O_2 sensor based on a glassy carbon (GC) electrode modified with carbon nanotubes functionalized (fCNTs) with a mixture of nanostructured TiO_2 and ZrO_2, using PB immobilized on the electrode surface as artificial peroxidase.

An electrochemical biosensor based on PB electrodeposited at a GC electrode modified with TiO_2.ZrO_2-fCNTs for the detection

TABLE 1 | Amount of reactants used in the synthesis of the nanostructured materials fCNT/MO_2(c)T.t.

Reactant	Nanostructural systems	
	fCNTs/TiO_2.ZrO_2 (100) T.t (*)	**fCNTs/TiO_2ZrO_2 (36)T.t (*)**
fCNT(g)	0.1500	0.080
Titanium isopropoxide T (mL)	0.3	0.3
Zirconium isopropoxide (mL)	0.4	0.4
Isopropanol (mL)	10.3	11.5
Propanol (mL)	–	–
Deionized wáter (mL)	0.14	0.16
Acetic acid (mL)	0.17	0.19

(*) (100) and (36) are wt% of CNTs wrt the metallic oxide, T is calcination temperature (80 or 500°C), and t is aging time (1 or 20 days).

of H_2O_2 has been reported for the first time here. The effect of covering the CNT walls with TiO_2-ZrO_2 nanoparticles is effective on the immobilization of PB, and the sensitivity of the electrochemical biosensor is studied.

2 MATERIALS AND METHODS

2.1 Reagents and Instrumentation

All solutions were prepared with distilled/deionized water (18 MΩ resistivity, Darmstadt, Germany). Carbon nanotubes were obtained from NANOCYL®NC7000(Austin, TX, USA). Nitric acid (HNO_3, 69.2 wt%) and hydrogen peroxide (H_2O_2 30% v/v) were purchased from Sigma-Aldrich (Darmstadt, Germany). Potassium phosphate monobasic (KH_2PO_4) and sodium hydroxide (NaOH, 99.9% p/p) were purchased from Fisher Scientific (Waltham, MA, USA). Phosphate-buffered saline (PBS: KH_2PO_4 + K_2HPO_4 + KCl, at different pH values) was used as a supporting electrolyte. Potassium ferricyanide ($K_3[Fe(CN)_6]$), iron trichloride hexahydrated ($FeCI_3 \cdot 6H_2O$), and potassium chloride (KCl) were obtained from BDH Chemicals (Philadelphia, PA, USA); hydrochloric acid (HCl, 37%) was from Fisher Scientific (Waltham, MA, USA); glassy carbon (GC, Φ = 3mm, geometric area = 0.0706 cm^2), silver/silver chloride reference electrode (Ag/AgCl), and graphite rod counter electrode were from CH Instruments (Austin, TX, USA); sulfuric acid (H_2SO_4, 98%) was from Fisher Scientific (Waltham, MA, USA); 1 μm, 0.3 μm, and 0.05 μm alumina powder were from CH Instruments (Austin, TX, USA); dimethylformamide (DMF) was from BDH Chemicals (Philadelphia, PA, USA); and poly (diallyldimethylammonium chloride) (PDDA, 4% w/w in water) was from Sigma.

2.2 Functionalization of Carbon Nanotubes

Functionalization of CNTs was carried out in order to insert functional groups on the CNT walls that allow the chemical interaction with other species. CNTs (NANOCYL®NC7000, Austin, TX, USA) of 90% purity were used, with an average diameter of 9.5 nm, transition metal content <1%, and surface area 250 m^2/g resistivity 10^{-4} Ωm. A previous pre-functionalization was carried out on the pristine CNTs using 3 mol L^{-1} HNO_3 and 1 mol L^{-1} H_2SO_4, under reflux at 80°C with constant agitation of 400 rpm for 6 h. The CNTs were washed, filtered, and dried (16 h) and finally gently crushed in a mortar and sieved. Then, the latter CNTs were functionalized employing an acid mixture HNO_3–H_2SO_4 (1:3) under reflux at 80°C for 30 min. Then, the functionalized multiwalled carbon nanotubes (fCNT) were washed with deionized water until neutral pH was reached and dried at 80°C for 10 h.

2.3 Synthesis of the fCNT/ TiO_2.ZrO_2–Nanostructured System

The nanostructured materials, fCNTs/TiO_2, fCNTs/ZrO_2, and fCNTs/TiO_2.ZrO_2, were obtained by *in situ* sol-gel synthesis of the metallic oxides (MO_2) on the fCNTs. The synthesis is based on that reported by Gonzalez et al. (2012). **Table 1** shows the number of reactants used. In summary, the following procedure was followed: a solution of titanium isopropoxide ($Ti(OPri)_4$) or/ and zirconium isopropoxide ($Zr(OPri)_4$) was prepared in 100 ml of isopropanol. This solution was gradually added to the fCNTs that were suspended in 100 ml of isopropanol under continuous agitation and left under reaction for 12 h. In addition, two different concentrations of fCNTs with respect to the metal oxides (MO_2) were used (36 and 100 w/w). The suspension was allowed to stand for 1–20 days at room temperature, the solvent was removed, and the material was dried under vacuum at 80°C for 4 h. The materials were calcined at two different temperatures 80 and 500°C for 2 h under argon atmosphere. The final product was ground to obtain a fine powder.

2.4 Characterization of the Nanomaterials

Transmission electron micrographs (TEMs) were taken using a JEOL 1220 microscope operating at an accelerating voltage of 100 kV. The samples were prepared by the wet suspension technique in an ethanol/water solution (70% v/v), and a drop of the suspension was placed on a TEM carbon–coated Cu grid.

Infrared spectra were acquired using a Nicolet iS10 FTIR spectrometer (Peabody, MA USA). The samples were prepared in KBr pellets. The frequency range was from 4,000 to 400 cm^{-1} with 64 scans at a resolution of 2 cm^{-1}.

X-ray diffraction patterns were obtained in a SIEMENS D5005 diffractometer (Radeberg, Germany) with a wavelength of 1.54178 Å in the range of 10°–80° 2θ degrees with a speed of 0.02/0.52 s.

Zeta potential was carried out for all the synthesized nanomaterials in Zetasizer Malvern Pananalytical equipment.

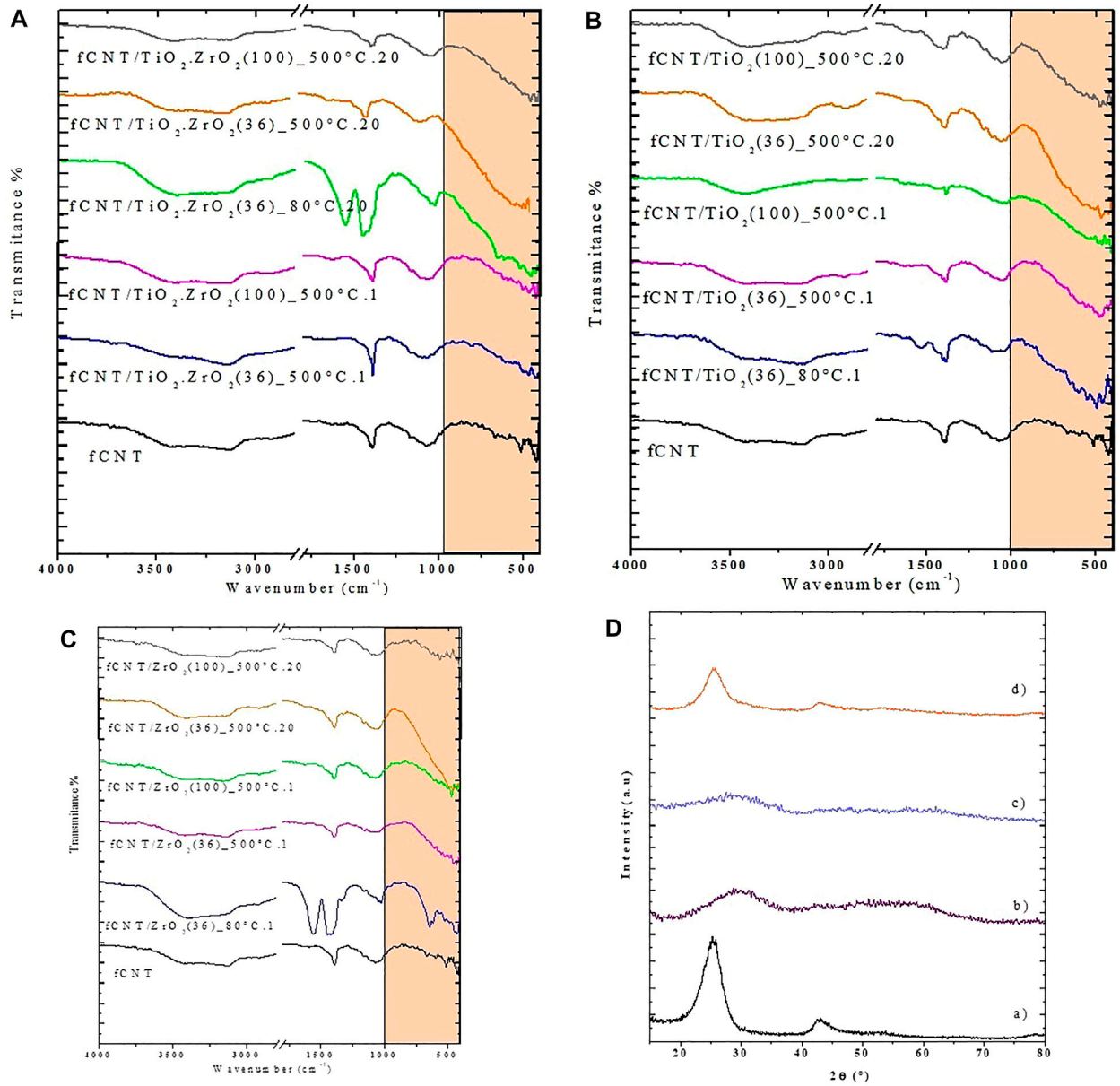

FIGURE 1 | FTIR spectra of the nanostructured materials obtained under different synthesis conditions: **(A)** fCNT/TiO_2ZrO_2; **(B)** fCNT/TiO_2; **(C)** fCNT/ZrO_2; and **(D)** XRD patterns of a) fCNT, b) ZrO_2 80°C, c) TiO_2- 80°C. and d) fCNT/TiO_2(36) 80. °C.1.

Measurements were performed on an aqueous suspension of carbon nanotube samples in distilled water as solvent. The environmental conditions of the analysis were a temperature of 24.1°C and a humidity of 45.7%. The samples were subjected to five measurement runs. From these data, the mean and standard deviation values of the zeta potential were calculated.

Differential scanning calorimetry and thermogravimetry analyses (DSC-TGA) were performed on a TA instrument SD Q600 ((TA Instrument, New Castle, DE, USA) from room temperature to 1,000°C, with a heating rate of 10°C/min under an air atmosphere.

The specific surface area was determined using the Brunauer–Emmett–Teller (BET) method in ASAP 2010 Micromeritics equipment (Micromeritics, Norcross (Atlanta, GA, USA). The samples were previously degassed under vacuum at 150°C for 4h, and the desorption isotherms were taken at liquid nitrogen temperature (77 K).

2.5 Glassy Carbon Electrode Modification

2.5.1 Cleaning of the Glassy Carbon Electrode

Mechanical polishing of the electrode was carried out with 0.5 and 0.03 μm alumina powder during 5 min, followed by an electrochemical cleaning using a potential from −1.2 to −1.6 V with a scan rate of 100 mV s^{-1} for 30 cycles.

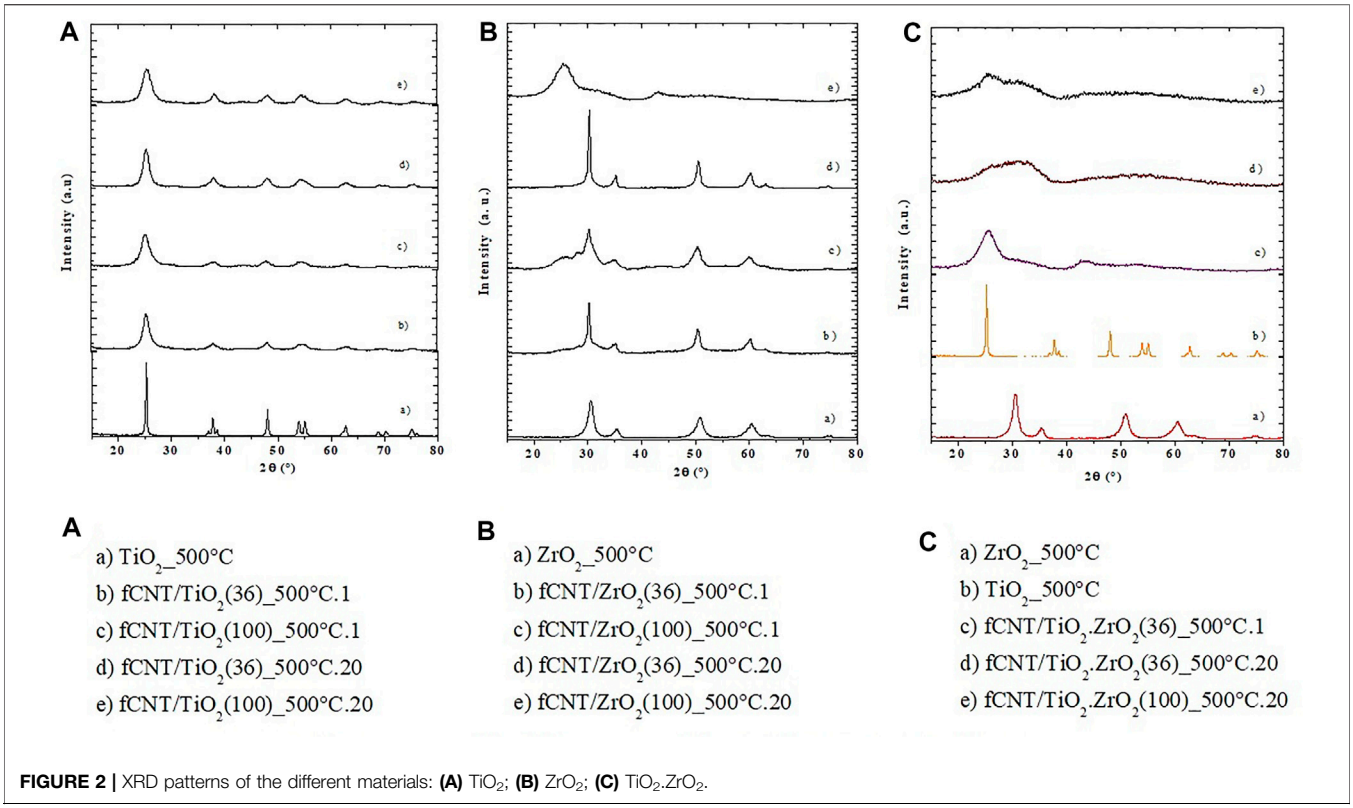

FIGURE 2 | XRD patterns of the different materials: **(A)** TiO_2; **(B)** ZrO_2; **(C)** $TiO_2.ZrO_2$.

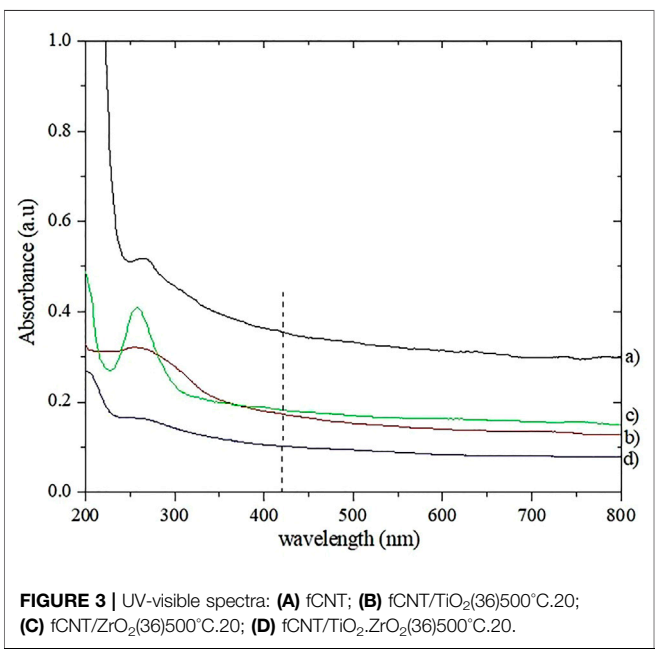

FIGURE 3 | UV-visible spectra: **(A)** fCNT; **(B)** fCNT/TiO_2(36)500°C.20; **(C)** fCNT/ZrO_2(36)500°C.20; **(D)** fCNT/$TiO_2.ZrO_2$(36)500°C.20.

2.5.2 Electrode Preparation of fCNTs/$TiO_2.ZrO_2$(c) T.t/GC

A suspension of fCNT/$TiO_2.ZrO_2$(c) T.t in DMF was prepared at a concentration of 5.0 mg mL^{-1} and sonicated during 1 h. This suspension was kept at 20°C. To modify the GC electrode, 10 µL of the fCNT/$TiO_2.ZrO_2$ suspension was added dropwise on its surface and was allowed to dry under infrared radiation for 20 min before use. In addition, electrodes of fCNTs/TiO_2(c) T.t/GC and fCNTs/ZrO_2(**c**)T.t/GC were prepared following an identical procedure.

2.5.3 Electrode Preparation of PB-fCNTs/$TiO_2.ZrO_2$ (c) T.t /GC

On the fCNTs/$TiO_2.ZrO_2$(c)T.t/GC electrode, 10 µL of the PDDA solution was pipetted and left to dry for 15 min at 50°C; subsequently the PB was electrodeposited on this surface. The electrodeposition of PB was achieved in an aqueous solution containing 2.5 mmol L^{-1} K_3 $[Fe(CN)_6]$ + 2.5 mmol L^{-1} $FeCl_3.6H_2O$ + 0.2 mol L^{-1} KCl + 0.2 mol^{-1} HCl, at a potential of +0.4 V for 240 s. Later, the PB-fCNTs/$TiO_2.ZrO_2$(c)T.t/GC electrode was activated by cycling at a potential range of −0.2 to 1.2 V at a sweep speed of 50 mV s^{-1} in 0.2 mol L^{-1} KCl + 0.2 mol L^{-1} HCl for eight cycles. The PB-fCNT/$TiO_2.ZrO_2$(c) T.t/GC electrode was left to dry at 50°C for 15 min, and then, a 10 µL volume of PDDA solution was dropped onto the modified electrode and dried for 15 min at 50°C.

2.6 Electrochemical Characterization of the Modified Electrodes

Experiments for the electrochemical characterization of the modified electrodes were carried out by cyclic voltammetry (CV) in a 0.1 mol L^{-1} PBS, in a range of a scan rate of

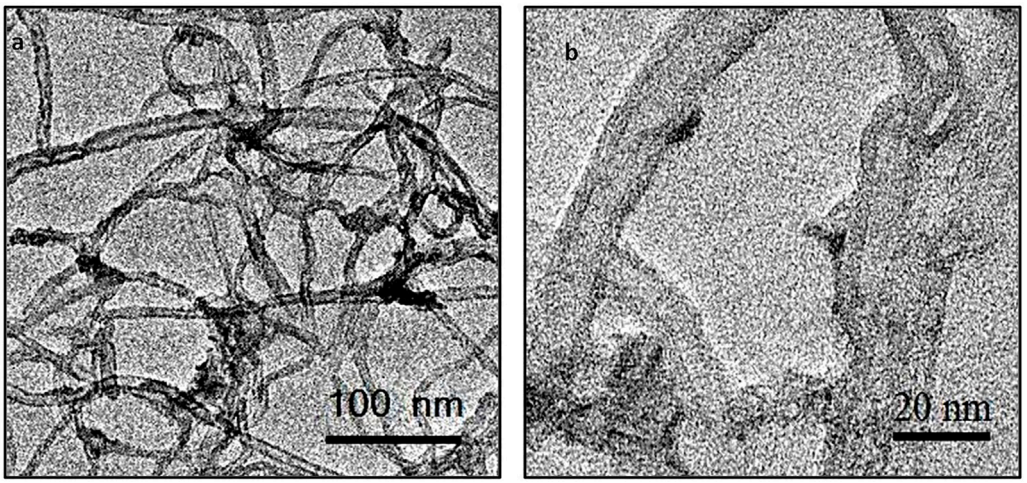

FIGURE 4 | TEMs of fCNT/TiO_2.ZrO_2(36)500°C.1: **(A)** general view and **(B)** detailed view of NPs on fCNT walls.

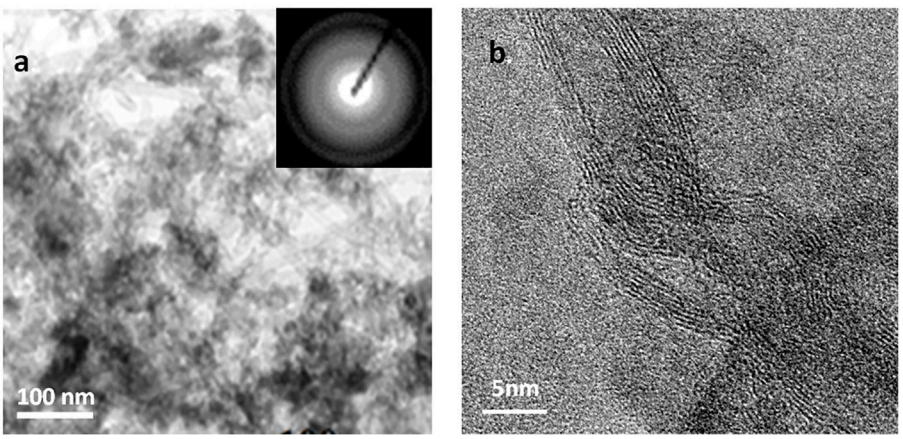

FIGURE 5 | TEMs of fCNT/TiO_2.ZrO_2(36)500°C.20: **(A)** general view showing Nps covering fCNTs; inset: electron diffraction pattern indicating the amorphous character of the Nps; **(B)** HRTEM showing Nps on fCNT walls.

10–120 mV s^{-1}. Using the Randles–Sevick equation (Ec.1), the diagnosis of the electrochemical process on the modified electrodes was carried out:

$$i_p = 2.69x10^5 n^{3/2} A C D^{1/2} v^{1/2} \quad (1)$$

where i_P (A) is the peak current, A is the electrode area in cm^2, C is the concentration of the species in solution (mol cm^{-3}), v is the potential scan rate (V s^{-1}), and D (cm^2 s^{-1}) is the diffusion coefficient.

Electrochemical capacitance of each modified electrode was obtained by CV in 0.1 mol L^{-1} PBS (pH 3.0) solution and at potentials of 0.20–0.55 V. According to the following equation (**Eq. 2**), we obtain

$$j = I_c/_A = C_{dl} v, \quad (2)$$

where C_{dl} (F) is the double layer capacitance, I_c is the current, and j (A cm^{-2}) is the current density.

Surface concentration of PB on the electrodes was calculated using the following equation (**Eq. 3**):

$$I_P = \frac{n^2 F^2 A v \Gamma C}{4RT}, \quad (3)$$

where n is the number of electrons transferred in the redox process, F is the Faraday's constant, R (J mol^{-1} K^{-1}) is the gas constant, T (K) is the temperature, A is the electrode area in cm^2, and v is the potential scan rate (V s^{-1}).

2.7 Hydrogen Peroxide Detection

Prior to obtention of the calibration plot for the quantification of H_2O_2, diagnostics tests were made through CV in order to determinate the response signal of the analyte in 0.1 mol L^{-1} PBS (pH 3.0) in a potential range from −0.40 to +0.60 V and a scan rate of 40 mV s^{-1}.

To evaluate the sensitivity and linearity of the response to H_2O_2 at the PB-fCNTs/TiO_2.ZrO_2(c)Tt/GC-modified electrode,

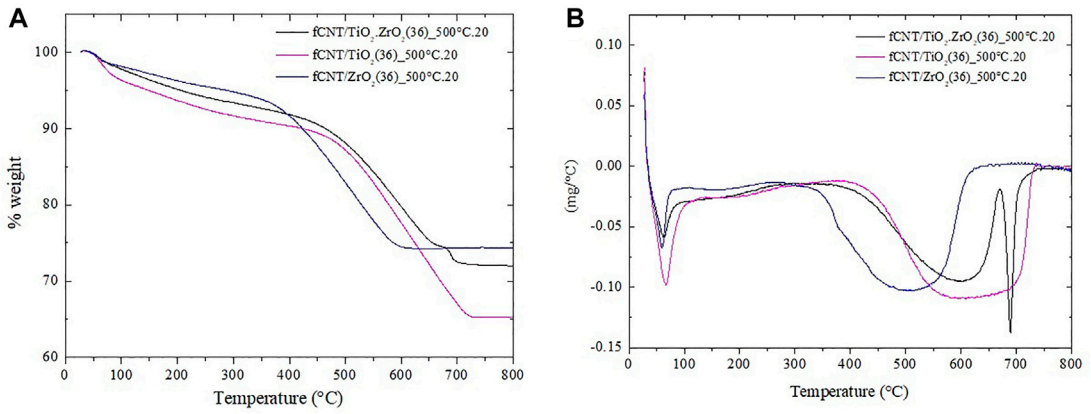

FIGURE 6 | Thermograms of nanostructured materials fCNT/MO_2(36)500°C.20: **(A)** TGA plot and **(B)** DTG plot.

chronoamperometric measurements were made in PBS, pH 3.0, with continuous stirring and adding aliquots of 0.05 mol L^{-1} H_2O_2 solution every 30 s to obtain a calibration plot from 150 to 1.028 μmol L^{-1}. The experiments were carried out keeping the temperature at 20°C ± 2.

2.7.1 Evaluation of the Determination of Hydrogen Peroxide in the Presence of Interferents

The selectivity of the PB-fCNTs/TiO_2.ZrO_2(c)T.t/GC electrode was evaluated by comparing the amperometric response of H_2O_2 before and after adding possible interferences in a PBS (pH 3.0). Ascorbic acids (15 mmol L^{-1}), glucose (15 mmol L^{-1}), and dopamine (20 mmol L^{-1}) were used as interferents; subsequently, chronoamperometric measurements were made in PBS (pH 3.0), by adding aliquots of 0.05 mol L^{-1} H_2O_2 every 20 s.

2.7.2 Evaluation of the Determination of Hydrogen Peroxide in Real Samples

For the application in a practical analysis, the PB-fCNTs/TiO_2.ZrO_2(c)T.t/GC electrode was used, and recovery percentages (R%) were calculated in fortified whey milk samples with different concentrations of H_2O_2 (250 μmol L^{-1} and 600 μmol L^{-1}).

3 RESULTS AND DISCUSSION

3.1 Characterization of the Nanostructured Materials

3.1.1 Fourier Transformed Infrared Spectroscopy

The FTIR spectra for the different synthesized materials are presented in **Figure 1**. Compared to the spectrum of the fCNTs (**Figures 1A–C**, black line spectrum), no great differences are observed for the materials aged for 1 day, suggesting that the titania and zirconia particles have not been formed yet or are too small. On the contrary, significant differences are observed for the materials aged for 20 days, especially in the region between 400 and 950 cm^{-1}. The materials fCNT/TiO_2.ZrO_2(36)500°C.20 and fCNT/TiO_2.ZrO_2(100)500°C.20 show an intense band in this region associated with Ti-O-Ti, Zr-O-Zr or Ti-O-Zr bonding. This band is also observed for the fCNT/TiO_2 and fCNT/ZrO_2 materials, suggesting a chemical interaction between the metal oxides and the fCNT walls. This suggests that the bonding for the fCNT/TiO_2.ZrO_2 material could be Ti-O-Zr. This broad band is located between that of fCNT/TiO_2 and fCNT/ZrO_2 (**Figures 1A–C**, spectrum in green and orange lines). The materials calcined at 80°C present bands similar to those found for uncalcined zirconia.

3.1.2 X-Ray Diffraction

The X-ray diffraction patterns of the synthesized materials under different conditions calcined for various periods at 80°C and at 500°C are presented in **Figures 1D**, **Figure 2**, respectively. The nanostructure materials calcined at 80°C (**Figure 1D**) do not show the reflexions corresponding to any metal oxide (ZrO_2, TiO_2, or TiO_2.ZrO_2), indicating that at this temperature crystallization has not taken place. The pure compounds aged at 500°C for 1 and 20 days present the characteristic peaks of anatase for the TiO_2 (JDPDS JCPDS84-1285), and the cubic phase of zirconia was formed for the ZrO_2 compound (JCPDS27-0997). These materials synthesized on fCNTs kept the same crystal structure with an average crystallite size, calculated by the Sherrer formula ($d = k\lambda/\beta \cos\theta$), of 5 nm for TiO_2/fCNT and 7.1 nm for the ZrO_2/fCNT (**Figures 2A,B**). The mixed compound TiO_2. ZrO_2/fCNT aged at 500°C showed an amorphous diffraction pattern (**Figures 2C–E**), indicating either amorphousness or too small nanoparticles that do not show sharp peak signals in the XRD pattern. The latter suggests that Zr_4^+ could suppress or delay the crystallization of the ZrO_2–TiO_2 system, and the growth rate is inhibited by the presence of both metal oxides. Similar results have been reported in the literature for the TiO_2–ZrO_2 system calcined in the range 400–550°C for ZrO_2 content over 50%; in our case, the ZrO_2 content is 60%. Therefore this is in good agreement with the results reported by different authors (Liu et al., 2003; Wan et al., 2004; Kitiyanan et al., 2006).

TABLE 2 | Thermogravimetric analysis.

	Temperature (°C)	Minimum DTG (°C)	Weight loss (%)	fCNT %
fCNT/TiO_2.ZrO_2 (36)500°C.20	33–100	63.20	2.20	25
	100–290	170.6	4.30	
	352–670	602.1	18.10	
	670–739	689.2	2.50	
fCNT/TiO_2.ZrO_2 (36)500°C.20	33–128	65	4.40	35
	128–337	210	4.10	
	370–740	–	25.40	
fCNT/TiO_2.ZrO_2 (36)500°C.20	33–97	58.0	1.80	28
	97–267	156.0	2.90	
	267–638	510.3	21.0	

TABLE 3 | Surface area BET of the nanostructured materials.

Material	BET area (m^2/G)	Mass% of fCNTs relative to oxide by TGA
fCNT	298.40 ± 2,72	100
fCNT/TiO_2.ZrO_2 (36)500°C.20	81.54 ± 1,13	25
fCNT/TiO_2 (36)500°C.20	147.02 ± 1,89	39
fCNT/ZrO_2 (36)500°C.20	92.12 ± 1,03	28

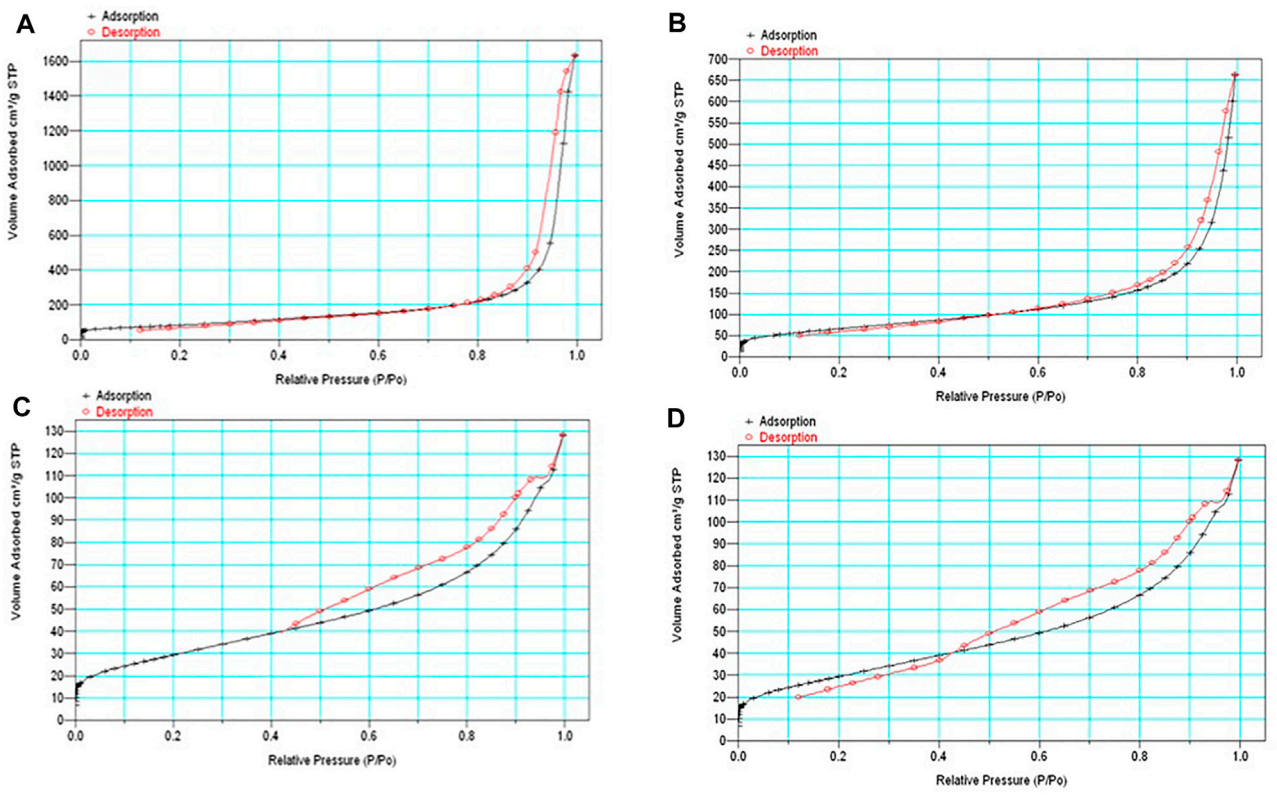

FIGURE 7 | N_2 adsorption–desorption isotherms: **(A)** fCNT, **(B)** fCNT/TiO_2.ZrO_2(36)500°C.20, **(C)** fCNT/TiO_2(36)500°C.20, and **(D)** fCNT/ZrO_2(36)500°C.20.

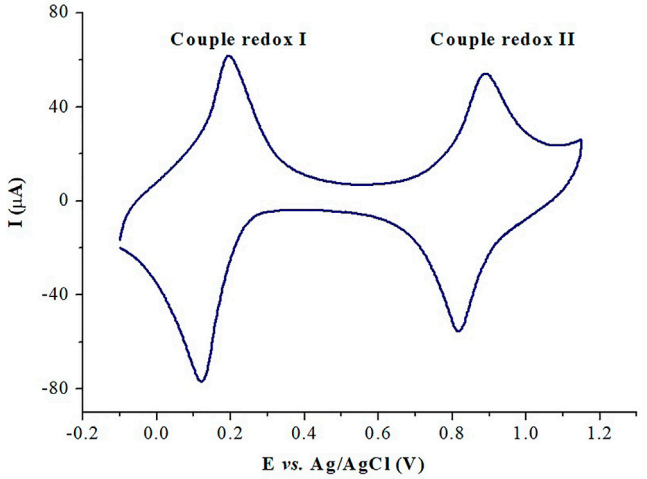

FIGURE 8 | Cyclic voltammetry of PB-fCNT/TiO_2.ZrO_2(36)500°C.20/GC-modified electrodes in PBS, pH 3.0 at 40 mVs^{-1}.

The results from FTIR and XRD showed that the fCNT/TiO_2.ZrO_2 (36)500°C.20 material presented the best performance; therefore, this material was chosen for the subsequent studies.

3.1.3 UV-Vis Spectroscopy

The UV-vis spectra of the nanostructure mixed oxide material fCNT/TiO_2.ZrO_2(36)500°C.20 is compared in **Figure 3** with the single metal oxides (MO_2) on carbon nanotubes: fCNT/TiO_2 (36) 500°C.20, fCNT/ZrO_2 (36)500°C.20, and the fCNT. It can be observed that the mixed oxide nanostructured material fCNT/TiO_2.ZrO_2(36)500°C.20 presents a lower absorption at 258 nm than the fCNT/MO_2 systems. This could be attributed to the very small particle size obtained for this material, as was observed by XRD. This agrees with the XRD patterns reported for the mixed TiO_2-ZrO_2 system reported by Kitiyanan et al. (2006).

3.1.4 Transmission Electron Micrographs

TEMs of the mixed oxide nanostructured materials calcined at 500°C and aged for 1 and 20 days (fCNT/TiO_2-ZrO_2 (36)500°C.1 and fCNT/TiO_2.ZrO_2 (36)500 °C.20 are shown in **Figures 4**, **5**, respectively. It can be observed that after 1 day, very few particles were formed (**Figure 4**), consistent with the FTIR and XRD results. However, after 20 days of aging (**Figure 5**), a large number of nanoparticles are observed covering the fCNT walls. **Figure 5A** is a general view of the material after 20 days of aging, showing a large number of nanoparticles, and the inset show the electron diffraction pattern indicating the amorphous characteristic of these nanoparticles. **Figure 5B** is a high-resolution electron microscopy (HREM) image of the same material showing the distribution of the nanoparticles on the fCNT walls.

3.1.5 Thermogravimetric Analysis

The fCNT/TiO_2.ZrO_2 (36)500°C.20 material loses 28 w%. This represents an intermediate weight loss compared with the fCNT/TiO_2(36)500°C.20 and fCNT/ZrO_2 (36)500°C.20 materials (**Figure 6**). In total, four stages of weight loss are observed: the first between 33 and 100°C with a minimum in the DTG at 63.2°C associated with desorbed water; the second stage between 100 and 290°C corresponds to remained amorphous carbon; the third stage between 352 and 670°C represents the degradation and decomposition of fCNT; and the fourth stage from 670 to 739°C presents a sharp minimum in the DTG plot at 689°C, associated to the crystallization of $TiZrO_4$. Zou and Lin (2004) reported minima values at 754, 712, and 606°C for TiO_2/ZrO_2 mixtures with ZrO_2 molar contents of 25, 50, and 75%, respectively. The molar ratio of ZrO_2 obtained in the present work should be near 60%, as was theoretically calculated; therefore the sharp minimum at 689°C would correspond to the crystallization of the ZrO_2-TiO_2 system with the formation of a new phase $ZrTiO_4$ (Zou and Lin, 2004). The latter is in good agreement with the ZrO_2–TiO_2 phase diagram (Troitzsch and Ellis, 2004). Furthermore, the final decomposition temperature of the fCNTs could be between 640 and 740°C. **Table 2** presents the different stages and the percentage of fCNTs with respect to the MO_2, which is slightly lower than the theoretical value, especially for the fCNT/TiO_2 (36)500°C.20 and fCNT/ZrO_2 (36) 500°C.20 materials. The minima values of the DTG curves for the fCNT/TiO_2.ZrO_2 (36)500°C.20 material are at intermediate positions compared with the fCNT/TiO_2 (36)500 °C.20 and fCNT/ZrO_2 (36)500°C.20 compounds.

3.1.6 Surface Area

The surface area of the nanostructured systems fCNT/TiO_2.ZrO_2 (36)500°C.20 is lower than that of fCNT/TiO_2 (36)500°C.20 and fCNT/ZrO_2 (36)500°C.20 (**Table 3** and **Figure 7**), attributed to the larger amount of TiO_2.ZrO_2 nanoparticles covering the fCNTs, therefore decreasing the surface area.

3.1.7 Electrochemical Characterization

Cyclic voltammetry was used to evaluate the electrochemical behavior of the PB-fCNT/TiO_2.ZrO_2 (36)500°C.20 film on the GC electrode. **Figure 8** shows the CV obtained for the PB-fCNT/TiO_2.ZrO_2 (36)500°C.20/GC electrode recorded at a scan rate of 40 $mV\,s^{-1}$ in PBS 0.1 $mol\,L^{-1}$ (pH 3) as a supporting electrolyte. The CV shows two well-defined redox couples, with potential $E_{1/2}$ ($E_{1/2}$= (E_{pa} + E_{pc})/2) for the redox couple I and II of 0.189 and 0.875 V (*vs.* Ag/AgCl), respectively; these values were independent of the scan rate. The redox couple I signal between 0.3 and −0.1 V is associated with high-spin redox reactions $Fe(CN)_6^{3-/4-}$ (the conversion of Prussian blue (PB) to Prussian white (PW) species, reaction 1), and the redox couple II signal between 0.7 and 1.1V corresponds to the reaction of low spin $Fe^{3+/2+}$ (Prussian blue (PB) to Berlin green (BG) species, reaction 2). The electrochemical behavior described of the PB on the electrode PB-fCNT/TiO_2.ZrO_2 (36)500°C.20/GC agrees with reports described in the literature for PB Nps (Li et al., 2007; Adekunle and Ozoemena, 2010; Cantanhêde Silva et al., 2010; Kong et al., 2015).

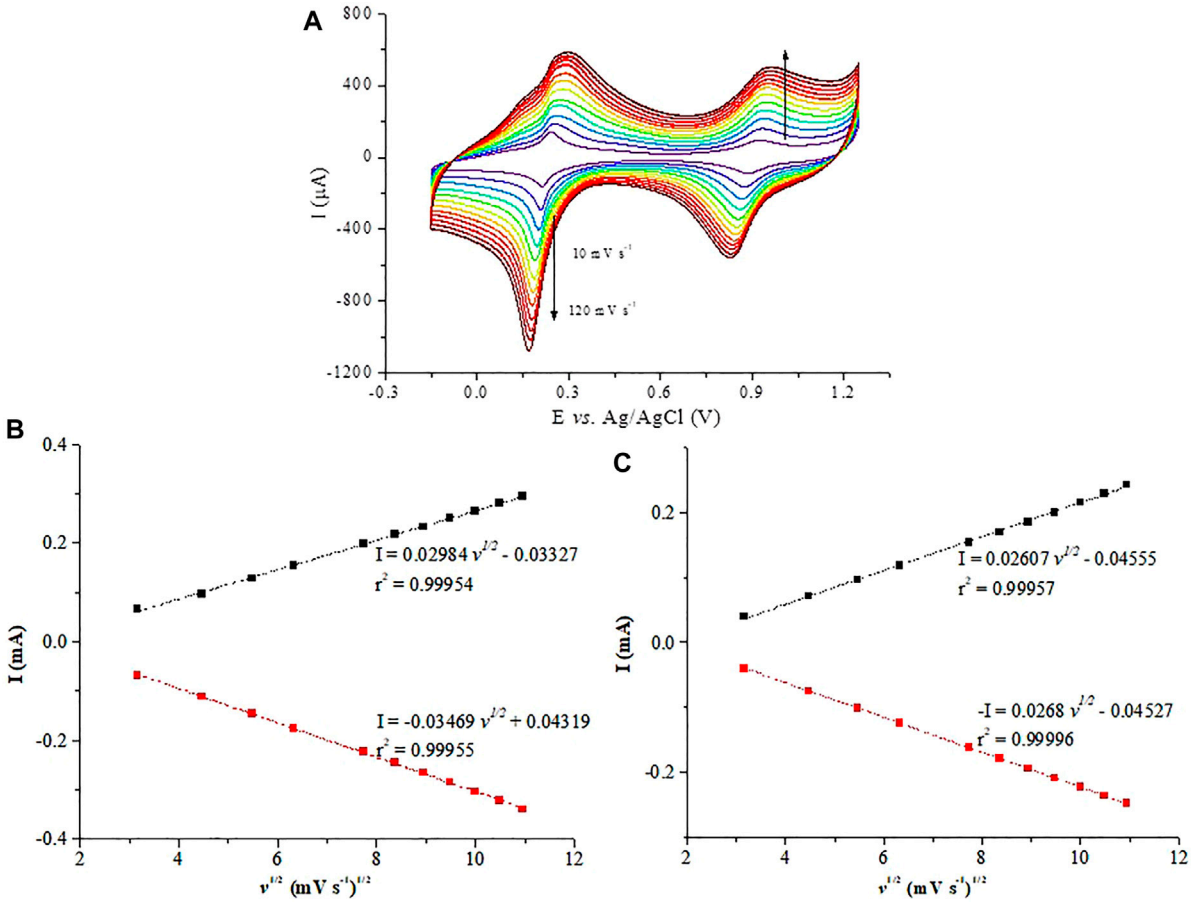

FIGURE 9 | (A) Cyclic voltammetry at PB-fCNT/TiO_2.ZrO_2(36)500°C.20/GC-modified electrode in PBS at pH 3.0 at different scan rates; **(B)** PB reduction; **(C)** PB oxidation peaks current vs. the square root of the scan rate, I vs. (v)1/2.

TABLE 4 | Comparison of the obtained electrochemical parameters for the PB-fCNT/TiO_2.ZrO_2 (36)500°C.20/GC electrode with the prepared electrodes under the same conditions with the individual oxides in their structure (Li et al., 2007; Rathee et al., 2021).

Parameter/Electrode	PB-fCNT/GC	PB-fCNT/TiO_2.ZrO_2 (36)500°C.20/GC	PB-fCNT/ZrO_2 (36)500°C.20/GC	PB-fCNT/TiO_2 (36)500°C.20/GC
$E_{1/2}$ (reduction/oxidation) /mV	0.22/0.88	0.23/0.90	0.23/0.90	0.23/0.87
Ipa/Ipc (reduction/oxidation)	0.86/1.13	0.80/0.90	0.79/1.6	0.88/1.44
Γ_c (mol cm^{-2})	3.98×10^{-10}	1.07×10^{-8}	1.2×10^{-9}	4.72×10^{-9}
Capacitance (mF cm^{-2})	2.37	2.96	1.51	1.48
k_s (s^{-1})	2.7×10^{-2}	8.47×10^{-5}	6.04×10^{-3}	8.70×10^{-4}

$$Fe_4^{III}[Fe^{II}(CN)_6]_3 + 4e^- + 4K^+ \rightleftarrows [K_4Fe_4^{II}(CN)_6]_3 \quad \text{(R1)}$$

PB PW

$$Fe_4^{III}[Fe^{II}(CN)_6]_3 + 4A^- + \rightleftarrows K_4Fe_4^{III}[Fe^{III}(CN)_6A]_3 + 3e^- \quad \text{(R2)}$$

PB, BG

For the PB-fCNT/TiO_2.ZrO_2 (36)500°C.20/GC-modified electrode, the voltammetry signals in the reduction zone show an Ipa/Ipc (peak anodic current /peak cathodic current) of 0.86, and the ΔEp (the separation of the peak potential) is 0.221 V, while in the oxidation zone, the ratio Ipa/Ipc is 0.95, and ΔEp is 0.151 V. These results suggest a quasi-reversible reaction process of PB on the surface of the modified electrode.

According to the Randles–Sevcik equation (Wang, 2000), **Figure 9** shows a linear plot of Ipc and Ipa versus $v^{1/2}$, for the PB-fCNT/TiO_2.ZrO_2 (36)500°C.20/GC electrode, revealing a diffusion-controlled process, which we have related to the slow diffusion of potassium ions in the lattice of the film on the electrode (Karyakin, 2001).

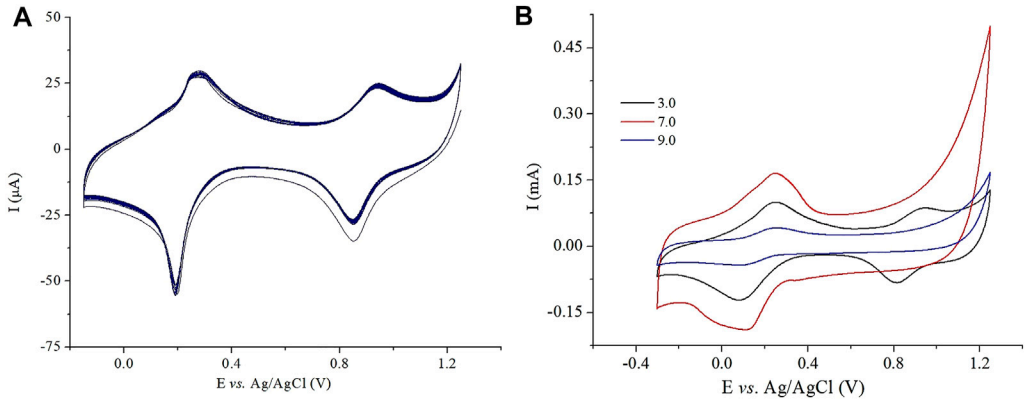

FIGURE 10 | Cyclic voltammetry at the PB-fCNT/TiO_2.ZrO_2(36)500°C.20/GC-modified electrode in **(A)** PBS (pH 3), 40 mV/s, and 90 cycles; **(B)** PBS, pH 3.0, 7.0, and 9.0.

The surface concentration (Γ_c) of PB on the modified electrode was evaluated from the slope I_p/A versus ν, according to the following equation (Tang et al., 1994; Du et al., 2010):

$$Ip = \frac{n^2F^2Av\Gamma c}{4RT} \quad (4)$$

where Ip is the current (A), A is the surface area of the electrode (cm $^{-2}$), ν is the potential scan rate (Vs^{-1}), n is the number of electrons, R is the gas constant (J mol^{-1} K^{-1}), T the temperature (K), and F the Faraday constant (C mol^{-1}). The average value of Γc or the redox peaks was 1.07×10^{-8} mol cm^{-2} (for n = 4 and ν < 500 mVs^{-1}). Γc for electrode PB-fCNT/TiO_2.ZrO_2 (36)500°C.20/GC is one order of greater magnitude than the prepared electrodes with metal oxides individually; PB-fCNT/ZrO_2 (36) 500°C.20/GC and PB-fCNT/TiO_2 (36)500 °C.20/GC are reported in the literature (Guerrero et al., 2019; Jerez-Masaquiza et al., 2020), **Table 4**. This result suggests that the oxides ZrO_2 and TiO_2 can act altogether in order to control PB nucleation either on the nanotubes, acting as a seed for PB film growth or as a "coating agent", resulting in a larger electroactive surface area for the PB growth on the electrode surface.

The electrochemical capacitance, C_{dl}, of the modified electrode was studied by CV, and this was carried out in PBS (pH 3.0) and potentials of 0.20–0.60 V (Haghighi et al., 2010). The following equation describes that the background current is a function of the scan rate:

$$j = I_c/A = C_{dl}\, v \quad (5)$$

where A is the effective surface area, ν is the scan rate, and C_{dl} is the electrochemical double-layer capacitance. Plot I_c/A versus ν presented a straight line where the C_{dl} of the modified electrode was obtained from the slope (data not shown). The C_{dl} obtained for PB-fCNT/TiO_2.ZrO_2 (36)500°C.20/GC was 2.96 mF cm^{-2}; this is a higher value than that reported for electrodes prepared under the same conditions with the individual oxides (MO_2), **Table 4**. This indicates that the PB-fCNT/TiO_2.ZrO_2(36)500°C.20/GC electrode has a larger specific area than individually modified electrodes with each oxide, which agrees with the results obtained by calculating the BET surface area.

Based on Laviron's theory (Zhang et al., 2003a; Lin et al., 2003), the electron transfer rate constant (k_s) was determined for the modified electrode in PBS (pH 3), measuring the variations of the anodic and cathodic potential peaks at different scan rates, when ΔEp was superior to 100/n mV. Assuming n = 4, the calculated value for ks was 5.47×10^{-5} s^{-1}, lower value than that reported for electrodes prepared under the same conditions with the individual oxides in their structure, **Table 4**, which suggests that the PB-fCNT/TiO_2 (36)500°C.20/GC electrode favors the electronic transfer on its surface.

The stability of the modified electrode PB-fCNT/TiO_2.ZrO_2 (36) 500°C.20/GC was tested by measuring the decrease of the voltammetry currents during the potential cycles. The electrode showed no decrease in the current in the supporting electrolyte (**Figure 10A**), when subjected to 90 cycles of potential from −0.15 to +1.25 V at a scan rate of 40 mV/s. We have associated the good stability of the electrode to the fact that the nanomaterial fCNT/TiO_2.ZrO_2 has good electrical conductivity, where the carbon atoms of the fCNT, as electron donors, and the CN of PB, as electron acceptors, present efficient π−π interaction (Shim et al., 2002; Zhang et al., 2003b; Lin et al., 2003); also, the iron cations in PB successfully interact with the carboxyl anions of fCNTs (Diao et al., 2002), thus generating an electrochemically efficient composite.

In addition, the stability of the modified electrode PB-fCNT/TiO_2.ZrO_2 (36)500°C.20/GC was evaluated by cyclic voltammetry at different pH values. **Figure 10B** shows the current intensity between the third and the first cycle at pH values ranging between 3.0.7.0 and 9.0. At pH 3.00, the electrode showed the best stability, with a slight decrease in current during cycles. At pH 9, a rapid decrease in current intensity is observed, which may be related to the formation of $Fe(OH)_3$ and the consequent decomposition of PB (Stilwell et al., 1992); at pH 7, well-defined PB to PW transformation peaks can be observed but the PB to BG transformation peaks are distorted until they disappear. As these results show, a very high stability of the electrode in acid solution was obtained, where pH 3.0 is considered as the most suitable value for the supporting electrolyte and the

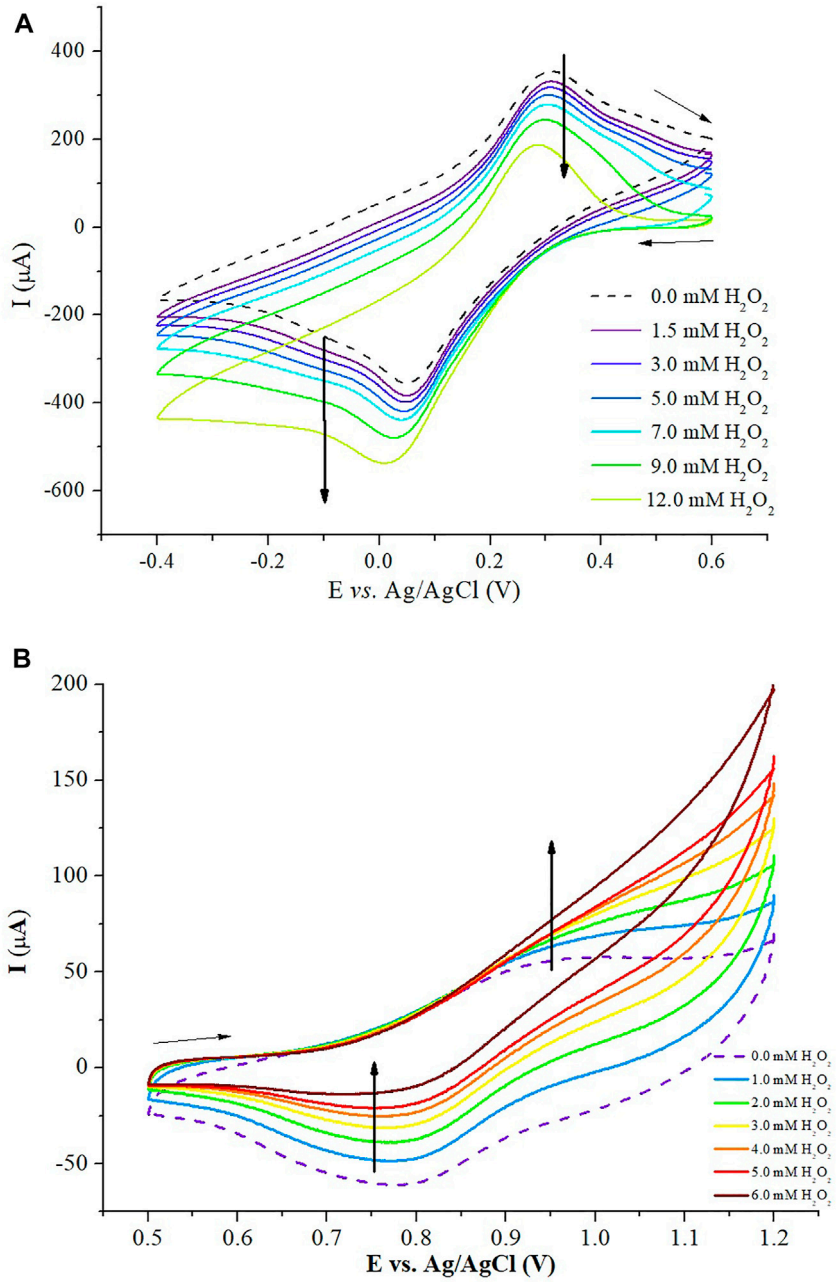

FIGURE 11 | (A) Cyclic voltammetry of H_2O_2 at the PB-fCNT/TiO_2.ZrO_2(36)500°C.20/GC-modified electrode (reduction zone) in 0.1 mol L^{-1} PBS (pH. 3.0) at 40 mV s^{-1}. **(B)** Cyclic voltammetry of H_2O_2 at the PB-fCNT/TiO_2.ZrO_2(36)500°C.20/GC-modified electrode (oxidation zone) in 0.1mol L^{-1} PBS (pH. 3.0) at 40 mV s^{-1}.

application of the PB-fCNT/TiO_2.ZrO_2 (36)500°C.20/GC electrode as a sensor of H_2O_2; therefore, this is the pH that was maintained for subsequent studies.

3.2 Electrocatalytic Behavior

Reduction of H_2O_2 at a PB-modified electrode surface has been shown to follow the classical two-electron reduction (reaction 3) (Sitnikova et al., 2014; Noël et al., 2016):

$$H_2O_2 + 2e^- \leftrightarrow 2HO^- \quad \text{(R3)}$$

where the loss of stability of the electrode is generally associated with the progressive loss of catalytic activity over time, which is attributed to the basification of the environment near the electrode surface by the production of OH^- ions in the reduction of H_2O_2 since PB is known to react with HO- according to the reaction (Montes et al., 2016) (Ricci et al., 2003):

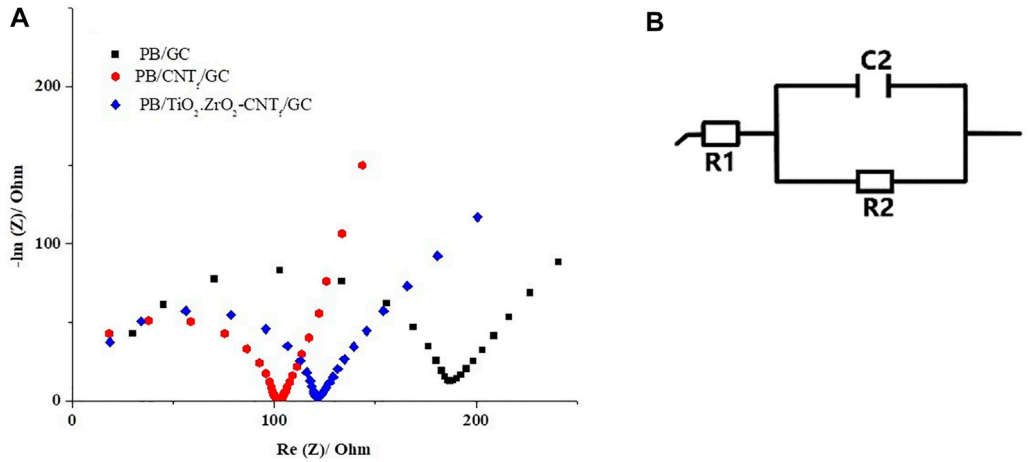

FIGURE 12 | (A) Nyquist plots: PB/GC, PB/fCNT/GC, and PB/TiO_2.ZrO_2- fCNT/GC-modified electrodes in 7.5 mmol L H_2O_2 in 0.1 mol 1.1 mol/L. PBS (pH 3.0). **(B)** Equivalent circuit of the three electrodes.

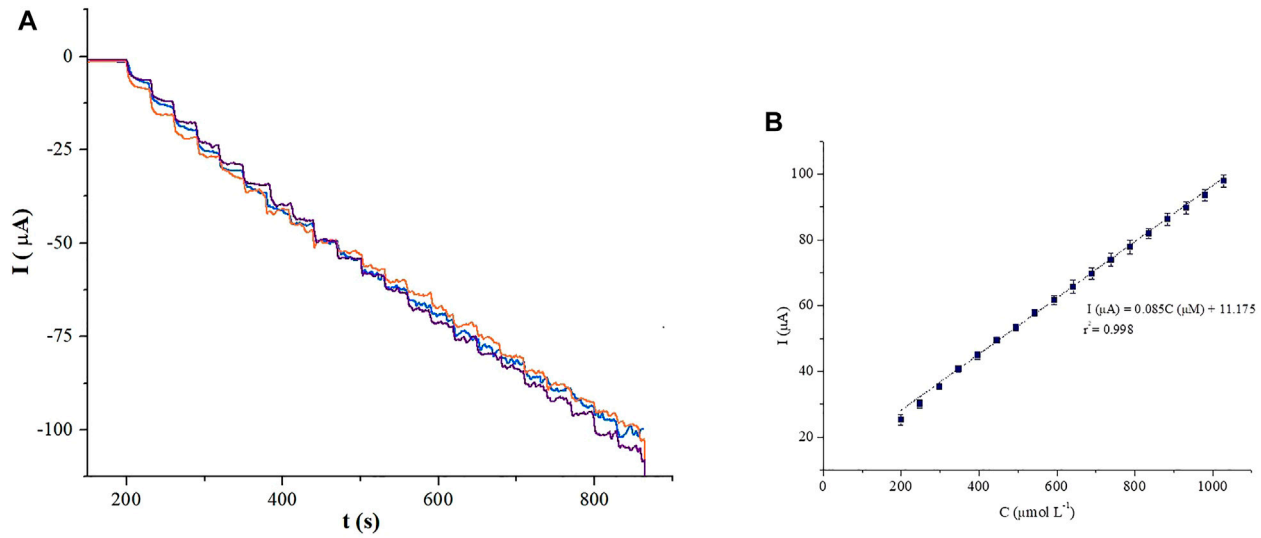

FIGURE 13 | Chronoamperometric detection of H_2O_2 at the PB-fCNT/TiO_2.ZrO_2(36)500°C.20/GC electrode, in PBS (pH 3) solution **(A)** and its **(B)** calibration plot. Working potential of –0.03 V vs. Ag/AgCl.

$$Fe_4^{III}\left[Fe^{II}(CN)_6\right]_3 + 12OH^- \rightarrow 4Fe(OH)_3 + 3\left[Fe^{II}(CN)_6\right]^{4-} \quad \text{(R4)}$$

For the case of the PB-fCNT/TiO_2.ZrO_2 (36)500°C.20 material, the obtained results for the Z potential (not shown) indicated that its surface is negatively charged, which can contribute to the repulsion of surface OH^- ions and thus increases the stability of the PB-fCNT/TiO_2.ZrO_2 film on the sensor surface.

To evaluate the catalytic activity of the electrode PB-fCNT/TiO_2.ZrO_2 (36)500°C.20/GC for H_2O_2, cyclic voltammograms were taken in the presence and absence of this analyte (**Figure 11**). In the presence of H_2O_2, both in the zone of conversion from PB to PW, reaction 1 (**Figure 11A**), and in the zone of conversion from PB to BG, reaction 2 (**Figure 11B**), it showed a decrease in reverse redox currents and an increase in forward redox currents, demonstrating that electrocatalytic reduction and oxidation, respectively, of H_2O_2 occurred on PB-fCNT/TiO_2.ZrO_2 (36)500°C.20/GC–modified electrode. The redox peaks in the voltammogram of **Figure 11B** show electrocatalysis toward the oxidation of H_2O_2 (R6), while the redox peaks in **Figure 11A** show the electrocatalysis of the reduction of H_2O_2 (R5).

The reduction reaction is as follows:

$$K_4Fe_4^{II}\left[Fe^{II}(CN)_6\right]_3 + 2H_2O_2 \rightleftarrows Fe_4^{III}\left[Fe^{II}(CN)_6\right]_3 + 4OH^- + 4K^+ \quad \text{(R5)}$$

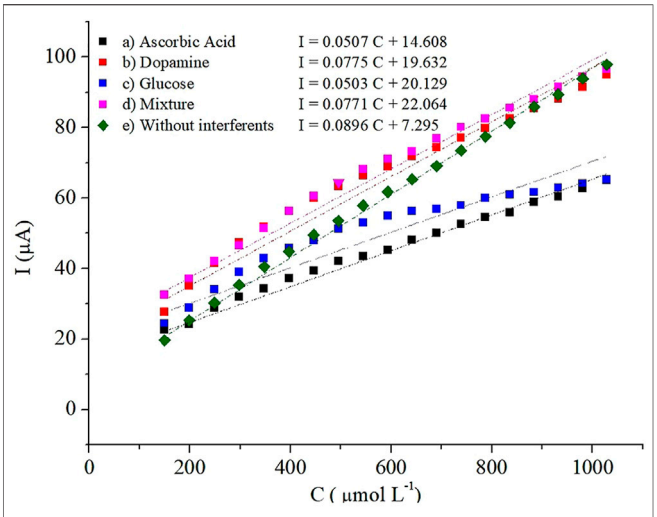

FIGURE 14 | Calibration plots of H_2O_2 at the PB-fCNT/TiO_2.ZrO_2(36) 500°C.20/GC electrode in PBS, pH 3 **(A)** with 10 mM of ascorbic acid; **(B)** 10 mM of dopamine; **(C)**10 mM of glucose; (D) 10 mM mixture of ascorbic acid, dopamine, and glucose; and (E) without interferents.

The oxidation reaction is as follows:

$$2Fe_4^{III}\left[Fe^{III}(CN)_6\right]_3 + A_3 + 3H_2O_2 \rightleftarrows 2Fe_4^{III}\left[Fe^{II}(CN)_6\right]_3 + 3O_2 + 6A^- + 6H^+ \quad \text{(R6)}$$

However, according to the voltammograms in **Figure 11A**, on the PB-fCNT/TiO_2.ZrO_2 (36)500°C.20/GC electrode, a better response was obtained for the electroreduction of H_2O_2 compared with the electrooxidation obtained in the voltammogram with the increase in peroxide concentration **Figure 11B**.

Electrochemical impedance spectra (EIS), from 40 KHz to 5 MHz, 0.01 Hz to 2 MHz, and 0.1 Hz to 5 MHz for PB/GC, PB/$_f$CNT/GC, and PB/TiO_2.ZrO_2-fCNT/GC electrodes, respectively, and an applied sinusoidal perturbation of 10 mV, in the presence of H_2O_2, were recorded. **Figure 12** shows the impedance spectra at 0.10 V (reduction of H_2O_2 potential) for PB/GC, PB/fCNT/GC, and PB/TiO_2.ZrO_2-fCNT/GC electrodes. At the PB/GC electrode (black curve), charge transfer resistance (Rct) at a high frequency is higher than for the other electrodes. Immobilization of PB/TiO_2.ZrO_2-fCNT films on the GC (red curve) produced the smallest semicircle, which demonstrated that PB/TiO_2.ZrO_2-fCNT/GC-modified electrodes have a higher Rct value than PB/GC and PB/fCNT/GC (blue curve); this implies that TiO_2.ZrO_2 nanoparticles play an important role in providing the conducting bridges for the charge transfer of H_2O_2 at PB/TiO_2.ZrO_2-fCNT/GC-modified electrode, in agreement with the literature (Yang et al., 2016).

To evaluate the rate constant, K_c, for the catalytic reaction, the current signals were used on the electrode PB-fCNT/TiO_2.ZrO_2 (36)500°C.20/GC in the presence (I_c) and in the absence of H_2O_2, (I_L), according to the following equation (Galus et al., 1976):

TABLE 5 | Recovery data for H_2O_2 in spiked milk serum samples over a PB-fCNT/TiO_2.ZrO_2 (36)500°C.20/GC sensor.

Sample	Spiked amount (μmol L^{-1})	Measured amount (n = 3) (μmol L^{-1})	Recovery (%)
Milk serum	250	282.21 ± 12.12	93.12
	550	561.92 ± 6.93	100.08

$$\frac{I_c}{I_L} = (K_c C\pi)^{1/2} t^{1/2} \quad (6)$$

where K_c, C, and t are the rate constant of the catalytic chemical reaction ($cm^3\ mol^{-1}\ s^{-1}$), concentration of H_2O_2 in the bulk of the solution ($mol\ cm^{-3}$), and the time (s), respectively. From the slope of the plot of I_c/I_L versus $t^{-1/2}$ (not shown), the K_c value for a fixed concentration of H_2O_2 was obtained. The average value of K_c (n = 3) in the concentration range of 150 at 1.028 μmol L^{-1} was 11.52 × 10^4 $cm^3\ mol^{-1}\ s^{-1}$, which is two orders of magnitude smaller than the values of ×10.7310^6 and 9.84 × 10^8 $cm^3\ mol^{-1}s^{-1}$ previously reported for the electrodes PB-fCNT/ZrO_2(36)500°C.20/GC and PB-fCNT/TiO_2 (36)500°C.20/GC, respectively (Guerrero et al., 2019; Jerez-Masaquiza et al., 2020).

3.3 Electroanalytic Behavior

Figure 13A shows the chronoamperometric response on the PB-fCNT/TiO_2.ZrO_2 (36)500°C.20/GC electrode, after adding 0.050 mmol/L of H_2O_2 in PBS (pH 3) at −0.03 V. A linear H_2O_2 signal on the PB-fCNT/TiO_2.ZrO_2 (36)500°C.20/GC electrode for a concentration range from 1,000 μmol L^{-1} was obtained, **Figure 13B**, with a quantification limit (QL) of 59.78 μmol L^{-1} and the detection limit (DL) of 17.93 μmol L^{-1}. The PB-fCNT/TiO_2.ZrO_2 (36)500°C.20/GC electrode amplified the hydrogen peroxide current ~100 times compared with the electrodes PB-fCNT/TiO_2 (36)500°C.20/GC (Guerrero et al., 2019), which could be attributed to the good synergy of the nano oxides together on electrocatalysis to reduce hydrogen peroxide. The PB encapsulation in the internal channels of fCNTs compared to PB on the external surface improves electrochemical properties (Yagi et al., 2004; Chen et al., 2007); this is why it is suggested that the electronic interaction between the d-orbital of Fe electron in PB and the inner surface of the modified fCNT improves the electrocatalytic performance of the PB complex on this electrode surface. Therefore, the huge increase of the current densities in the presence of H_2O_2 on the PB-fCNT/TiO_2.ZrO_2 (36)500°C.20/GC electrode could also be attributed to the supramolecular electronic interactions between PB and the fCNT. On the other hand, according to the previous results (Guerrero et al., 2019), the PB-fCNTs/GC electrode showed an unstable behavior at the applied potentials for H_2O_2 detection. The comparison between the fCNT/TiO_2.ZrO_2 (36)500°C.20/GC electrode with the one previously reported for the PB-fCNT/ZrO_2 (36)500°C.20/GC electrode (Jerez-Masaquiza et al., 2020) has not been carried out since the latter, besides working on a different redox zone, presented issues for its optimal preparation. Therefore, the modified electrode fCNT/TiO_2.ZrO_2 (36)500°C.20/GC was considered the best electrode for the evaluation of the of H_2O_2 detection in operability terms.

TABLE 6 | Comparison of the results obtained at modified electrodes with other electrodes reported in the literature.

Modified electrode	Detection limit (mM)	Detection potential (V)	References
PB-fCNT/TiO_2.ZrO_2 (36)500°C.20/GC	1.79×10^{-2}	–0.03	This work
Paper-based electrochemical sensing platform	4.0	0.00	Kaumal et al. (2021)
Hematite (α-Fe_2O_3) nanoarrays on fluorine-doped SnO_2 glass (FTO)	2.0×10^{-2}	–1.50	Lv et al. (2022)
Au/stainless-steel	3.97×10^{-2}	–0.60	Huo et al. (2022)
Hybrid material–based polyaniline, dialdyhayed carboxmethyl cellouse, and in the presence of ZnO nanoparticles abbreviated	450	—	Althomali et al. (2022)
Silver nanoparticles (Ag NPs) entrenched in a silicate matrix (APS(SG))	2.5×10^{-2}	–0.40	Maduraiveeran et al. (2018)
Gold nanocubes embedded biocompatible hybrid hydrogels	15	–0.15	Manickam et al. (2020)

To assess the reproducibility response of the modified electrode PB-fCNT/TiO_2.ZrO_2 (36)500°C.20/GC, 10 (Lv et al., 2020) electrodes were made from the same GC electrode and independently showed acceptable reproducibility in the current value with relative standard deviation of 5.39% for 100 μmol L^{-1} H_2O_2. When the modified electrodes were not in use, they were stored in PBS (pH 3.0) at 4°C. In order to examine long-term storage stabilities, the voltammetric responses of the modified electrodes in 100 μmol L^{-1} H_2O_2 were monitored in regarding to storage time, every 5 days. After a storage period of 30 days, the PB-fCNT/TiO_2.ZrO_2 (36)500°C.20/GC electrode still retained the 78% of its initial current response to H_2O_2, indicating that the electrode has good stability and reproducibility.

When a sensor is used for the determination of H_2O_2 in samples such as whey milk, the anti-interference capacity is an important parameter because coexisting species such as glucose (Glu), ascorbic acid (AA), and dopamine (DA) can interfere with the determination of H_2O_2. **Figure 14** shows the calibration graphic for the electrocatalytic reduction of H_2O_2 by chronoamperometry at –0.03 V on the PB-fCNT/TiO_2.ZrO_2 (36)500°C.20/GC electrode in the presence of interfering species, including glucose (Glu), ascorbic acid (AA), dopamine (DA), and a mixture of them. The addition of individual species affected the electrode sensitivity in the following order: AA> Glu >DA; however, when all interferents are present in the solution, the sensitivity was not considerably affected.

Due to these results, the modified electrode PB-fCNT/TiO_2.ZrO_2 (36)500°C.20/GC was applied in the detection of hydrogen peroxide in whey milk samples. The accuracy of the developed analytical method was evaluated by calculating the recovery percentage (R%) in whey milk samples spiked with a known concentration of H_2O_2. **Table 5** shows that the values for R% range between 94 and 104%; these values agree with a good accuracy of the method.

Table 6 shows a comparison between the PB-fCNT/TiO_2.ZrO_2 (36)500°C.20/GC electrode and other electrodes reported in the literature. Table shows that our results are in agreement with other reports, suggesting that this electrode coating can be used to sense H_2O_2.

4 CONCLUSION

An electrochemical sensor for H_2O_2 detection, PB-fCNT/TiO_2.ZrO_2 (36)500°C.20/GC, was efficiently designed with fCNT/TiO_2.ZrO_2–modified GC electrode. TiO_2.ZrO_2 nanoparticles on fCNTs were successfully prepared. From the XRD, DTG, and TEM/electron diffraction analysis, we could see that amorphous nanoparticles of TiO_2.ZrO_2 were formed on the fCNT walls, where Zr^{4+} suppresses or delays the crystallization of the ZrO_2-TiO_2 system. The calculated value for the electron transfer rate constant (k_s) was lower than that reported for electrodes prepared under the same conditions with the individual oxides in their structure, which suggests that the PB-fCNT/TiO_2.ZrO_2 (36)500°C.20/GC electrode favors the electronic transfer at the PB–fCNT/GC electrode. Furthermore, the PB-fCNT/TiO_2.ZrO_2 layer exhibits good compatibility and affinity to the PB layer. The applicability of the sensor for detection of the hydrogen peroxide electrode was demonstrated in whey milk samples. Based on these advantages, the fabricated sensor exhibits good electrochemical sensibility, reversibility, and excellent linear relationship; nonetheless, the detection limit of the electrode can be improved. Finally, the fCNT/TiO_2.ZrO_2 layer can be used in the development of enzyme-based biosensors, which is the basis for future studies in our laboratory.

DATA AVAILABILITY STATEMENT

The raw data supporting the conclusions of this article will be made available by the authors, without undue reservation.

AUTHOR CONTRIBUTIONS

Conceptualization: LF, PE-M, and GG; methodology: LF, PE-M, and GG; validation: JA-P and DB-M; formal analysis: GG and LF; investigation: GG, LF, and PE-M; resources: RU, JP, and LC; data curation: JA-P and DB-M; writing—original draft preparation: LF, GG, and PE-M; writing—review and editing: LF and PE-M; visualization: LF, GG, and PE-M; supervision: LF, GG, and PE-M; project administration: RU and LC; and funding acquisition: RU.

FUNDING

This research was funded by the project EPN-PIMI 20-05: "Desarrollo de un biosensor electroquímico enzimático mediante nanotubos de carbono funcionalizados con mezclas de TiO_2 y ZrO_2 para la detección de H_2O_2," Escuela Politécnica Nacional, Quito, Ecuador.

ACKNOWLEDGMENTS

The authors would like to thank the Pontifical Catholic University of Ecuador and CEDIA (Corporation Ecuadorian for the Development of the Research and the Academy) for the technical support.

REFERENCES

Adekunle, A. S., and Ozoemena, K. I. (2010). Electrocatalytic Oxidation of Diethylaminoethanethiol and Hydrazine at Single-Walled Carbon Nanotubes Modified with Prussian Blue Nanoparticles. *Electroanalysis* 22 (21), 2519–2528. doi:10.1002/elan.201000289

Althomali, R. H., Alamry, K. A., Hussein, M. A., and Guedes, R. M. (2022). Hybrid PANI@dialdehyde Carboxymethyl cellulose/ZnO Nanocomposite Modified Glassy Carbon Electrode as a Highly Sensitive Electrochemical Sensor. *Diam. Relat. Mater.* 122, 108803. doi:10.1016/j.diamond.2021.108803

Bai, J., and Zhou, B. (2014). Titanium Dioxide Nanomaterials for Sensor Applications. *Chem. Rev.* 114 (19), 10131–10176. doi:10.1021/cr400625j

Cantanhêde Silva, W., Guix, M., Alarcón Angeles, G., and Merkoçi, A. (2010). Compact Microcubic Structures Platform Based on Self-Assembly Prussian Blue Nanoparticles with Highly Tuneable Conductivity. *Phys. Chem. Chem. Phys.* 12 (47), 15505–15511.

Chen, W., Pan, X., and Bao, X. (2007). Tuning of Redox Properties of Iron and Iron Oxides via Encapsulation within Carbon Nanotubes. *J. Am. Chem. Soc.* 129 (15), 7421–7426. doi:10.1021/ja0713072

Diao, P., Liu, Z., Wu, B., Nan, X., Zhang, J., and Wei, Z. (2002). Chemically Assembled Single-Wall Carbon Nanotubes and Their Electrochemistry. *ChemPhysChem* 3 (10), 898–991. doi:10.1002/1439-7641(20021018)3:10<898::aid-cphc898>3.0.co;2-u

Du, D., Wang, M., Qin, Y., and Lin, Y. (2010). One-step Electrochemical Deposition of Prussian Blue-Multiwalled Carbon Nanotube Nanocomposite Thin-Film: Preparation, Characterization and Evaluation for H2O2sensing. *J. Mat. Chem.* 20 (8), 1532–1537. doi:10.1039/b919500a

Galus, Z. (1976). "Fundamentals of Electrochemical Analysis [Internet]," In *Zitelli Davis' Atlas Pediatr. Phys. Diagnosis. Pol.* Editors R. A. Chalmers, and W. A. J. Brice. 2nd ed. (Boca Ratòn, NW: Ellis Horwood), 206, 387–407. Available at; https://www.crcpress.com/Fundamentals-of-Picoscience/Sattler/p/book/9781466505094#googlePreviewContainer.

Gonzalez, G., Albano, C., Herman, V., Boyer, I., Monsalve, A., and Brito, J. A. (2012). *Nanocomposite Building Blocks of TiO 2 – MWCNT F and ZrO 2 – MWCNT F*, 4.

Grisham, M. B. (2013). Methods to Detect Hydrogen Peroxide in Living Cells: Possibilities and Pitfalls. *Comp. Biochem. Physiology Part A Mol. Integr. Physiology* 165 (4), 429–438. doi:10.1016/j.cbpa.2013.02.003

Guerrero, L. A., Fernández, L., González, G., Montero-Jiménez, M., Uribe, R., Díaz Barrios, A., et al. (2019). Peroxide Electrochemical Sensor and Biosensor Based on Nanocomposite of TiO2 Nanoparticle/Multi-Walled Carbon Nanotube Modified Glassy Carbon Electrode. *Nanomaterials* 10 (1), 64. doi:10.3390/nano10010064

Gutiérrez, A., Rodríguez, M. C., Galicia, L., and Rivas, G. A. (2011). Amperometric Glucose Biosensor Electrode Modified with Carbon Nanotubes. doi:10.1149/1.3660633

Haghighi, B., Hamidi, H., and Gorton, L. (2010). Electrochemical Behavior and Application of Prussian Blue Nanoparticle Modified Graphite Electrode. *Sensors Actuators B Chem.* 147 (1), 270–276. doi:10.1016/j.snb.2010.03.020

Hou, Y. Y., Xu, J., Wang, F. T., Dong, Z., Tan, X., Huang, K. J., et al. (2021). Construction of an Integrated Device of a Self-Powered Biosensor and Matching Capacitor Based on Graphdiyne and Multiple Signal Amplification: Ultrasensitive Method for MicroRNA Detection. .doi:10.1021/acs.analchem.1c03521

Huo, D., Li, D., Xu, S., Tang, Y., Xie, X., Li, D., et al. (2022). Disposable Stainless-Steel Wire-Based Electrochemical Microsensor for *In Vivo* Continuous Monitoring of Hydrogen Peroxide in Vein of Tomato Leaf. *Biosens. (Basel)* 12 (1). doi:10.3390/bios12010035

Itaya, K., Shoji, N., and Uchida, I. (1984). Catalysis of the Reduction of Molecular Oxygen to Water at Prussian Blue Modified Electrodes. *J. Am. Chem. Soc.* 106 (12), 3423–3429. doi:10.1021/ja00324a007

Jerez-Masaquiza, M. D., Fernández, L., González, G., Montero-Jiménez, M., and Espinoza-Montero, P. J. (2020). Electrochemical Sensor Based on Prussian Blue Electrochemically Deposited at ZrO2 Doped Carbon Nanotubes Glassy Carbon Modified Electrode. *Nanomaterials* 10 (7), 1328. doi:10.3390/nano10071328

Karyakin, A. A. (2001). Prussian Blue and its Analogues: Electrochemistry and Analytical Applications. *Electroanalysis* 13 (10), 813–819. doi:10.1002/1521-4109(200106)13:10<813::aid-elan813>3.0.co;2-z

Karyakin, A. A., Puganova, E. A., Budashov, I. A., Kurochkin, I. N., Karyakina, E. E., Levchenko, V. A., et al. (2004). Prussian Blue Based Nanoelectrode Arrays for H2O2 Detection. *Anal. Chem.* 76 (2), 474–478. doi:10.1021/ac034859l

Karyakin, A., Karyakina, E., and Gorton, L. (1996). Prussian-Blue-based Amperometric Biosensors in Flow-Injection Analysis. *Talanta* 43 (9), 1597–1606. doi:10.1016/0039-9140(96)01909-1

Kaumal, M. N., Nissanka, N. A. A. B., and Perera Lh, R. (2021). Low Cost Paper-Based Electrochemical Sensing Platform for the Determination of Hydrogen Peroxide. *Curr. Appl. Sci. Technol.* 22 (2), 1–11. doi:10.55003/cast.2022.02.22.004

Kitiyanan, A., Sakulkhaemaruethai, S., Suzuki, Y., and Yoshikawa, S. (2006). Structural and Photovoltaic Properties of Binary TiO2-ZrO2 Oxides System Prepared by Sol-Gel Method. *Compos. Sci. Technol.* 66 (10), 1259–1265. doi:10.1016/j.compscitech.2005.10.035

Kong, B., Selomulya, C., Zheng, G., and Zhao, D. (2015). New Faces of Porous Prussian Blue: Interfacial Assembly of Integrated Hetero-Structures for Sensing Applications. *Chem. Soc. Rev.* 44 (22), 7997–8018. doi:10.1039/c5cs00397k

Li, H., Liu, Y., Wang, L., Sheng, K., Zou, L., and Ye, B. (20182018). Electrochemical Behavior of Diosmin and its Sensitive Determination on ZrO2-NPs-Coated Poly(diallyldimethylammonium Chloride)-Functionalized Graphene Modified Electrode. *Microchem. J.* 143, 430–440. doi:10.1016/j.microc.2018.08.023

Li, P., Wu, L., Li, B., Zhao, Y., and Qu, P. (2016). Highly Water-Dispersible Silver Sulfadiazine Decorated with Polyvinyl Pyrrolidone and its Antibacterial Activities. *Mater. Sci. Eng. C* 60, 54–59. doi:10.1016/j.msec.2015.11.021

Li, Z., Chen, J., Li, W., Chen, K., Nie, L., and Yao, S. (2007). Improved Electrochemical Properties of Prussian Blue by Multi-Walled Carbon Nanotubes. *J. Electroanal. Chem.* 603 (1), 59–66. doi:10.1016/j.jelechem.2007.01.021

Lin, Y., Zhou, B., Shiral Fernando, K. A., Liu, P., Allard, L. F., and Sun, Y.-P. (2003). Polymeric Carbon Nanocomposites from Carbon Nanotubes Functionalized with Matrix Polymer. *Macromolecules* 36 (19), 7199–7204. doi:10.1021/ma0348876

Liu, H., Guo, K., Duan, C., Dong, X., and Gao, J. (2017). Hollow TiO2 Modified Reduced Graphene Oxide Microspheres Encapsulating Hemoglobin for a Mediator-free Biosensor, *Biosens. Bioelectron.*, 87, 473–479. doi:10.1016/j.bios.2016.08.089

Liu, S. W., Song, C. F., Lü, M. K., Gu, F., Wang, S. F., Xu, D., et al. (2003). Structure and Photoluminescence Properties of xZrO2-(1 - x)TiO2 Composite Nanocrystals. *Mater Sci. Eng. B Solid-State Mater Adv. Technol.* 104 (1–2), 49–53. doi:10.1016/s0921-5107(03)00282-4

Lv, J., Fan, M., Zhang, L., Zhou, Q., Wang, L., Chang, Z., et al. (2022). Photoelectrochemical Sensing and Mechanism Investigation of Hydrogen Peroxide Using a Pristine Hematite Nanoarrays. *Talanta* 237, 122894. doi:10.1016/j.talanta.2021.122894

Lv, S., Zhang, K., Zhu, L., and Tang, D. (2020). Zif-8-assisted Nayf4:yb,tm@zno Converter with Exonuclease Iii-Powered Dna Walker for Near-Infrared Light Responsive Biosensor. *Anal. Chem.* 92 (1), 1470–1476. doi:10.1021/acs.analchem.9b04710

Maduraiveeran, G., Kundu, M., and Sasidharan, M. (2018). Electrochemical Detection of Hydrogen Peroxide Based on Silver Nanoparticles via Amplified Electron Transfer Process. *J. Mater Sci.* 53, 8328–8338. doi:10.1007/s10853-018-2141-7

Manickam, P., Vashist, A., Madhu, S., Sadasivam, M., Sakthivel, A., Kaushik, A., et al. (2020). Gold Nanocubes Embedded Biocompatible Hybrid Hydrogels for Electrochemical Detection of H2O2. *Bioelectrochemistry [Internet*, 131, 107373. doi:10.1016/j.bioelechem.2019.107373
Gold Nanocubes Embedded Biocompatible Hybrid Hydrogels for Electrochemical Detection of H2O2*Bioelectrochemistry*

Montes, R., Céspedes, F., and Baeza, M. (2016). Highly Sensitive Electrochemical Immunosensor for IgG Detection Based on Optimized Rigid Biocomposites. *Biosens. Bioelectron.* 78, 505–512. doi:10.1016/j.bios.2015.11.081

Noël, J. M., Médard, J., Combellas, C., and Kanoufi, F. (2016). Prussian Blue Degradation during Hydrogen Peroxide Reduction: A Scanning Electrochemical Microscopy Study on the Role of the Hydroxide Ion and Hydroxyl Radical. *ChemElectroChem* 3 (7), 1178–1184.

Rathee, G., Bartwal, G., Rathee, J., Mishra, Y. K., Kaushik, A., and Solanki, P. R. (2021). Emerging Multimodel Zirconia Nanosystems for High-Performance Biomedical Applications. *Adv. NanoBio Res.* 1 (9), 2100039. doi:10.1002/anbr.202100039

Rhee, S. G., Chang, T.-S., Jeong, W., and Kang, D. (2010). Methods for Detection and Measurement of Hydrogen Peroxide inside and outside of Cells. *Mol. Cells* 29 (6), 539–549. doi:10.1007/s10059-010-0082-3

Ricci, F., Amine, A., Moscone, D., and Palleschi, G. (2003). Prussian Blue Modified Carbon Nanotube Paste Electrodes: A Comparative Study and a Biochemical Application. *Anal. Lett.* 36 (9), 1921–1938. doi:10.1081/al-120023622

Roushani, M., Abdi, Z., Daneshfar, A., and Salimi, A. (2013). Hydrogen Peroxide Sensor Based on Riboflavin Immobilized at the Nickel Oxide Nanoparticle-Modified Glassy Carbon Electrode. *J. Appl. Electrochem* 43 (12), 1175–1183. doi:10.1007/s10800-013-0603-9

Roushani, M., and Dizajdizi, B. Z. (2015). Development of Nonenzymatic Hydrogen Peroxide Sensor Based on Catalytic Properties of Copper nanoparticles/Rutin/MWCNTs/IL/Chit. *Catal. Commun.* 69, 133–137. doi:10.1016/j.catcom.2015.06.004

Roushani, M., and Dizajdizi, B. Z. (2016). Development of Nonenzymatic Hydrogen Peroxide Sensor Based on Successive Pd-Ag Electrodeposited Nanoparticles on Glassy Carbon Electrode. *Electroanalysis* 28 (4), 787–793. doi:10.1002/elan.201500569

Roushani, M., and Karami, E. (2014). Electrochemical Detection of Persulfate at the Modified Glassy Carbon Electrode with Nanocomposite Containing Nano-Ruthenium Oxide/thionine and Nano-Ruthenium Oxide/celestine Blue. *Electroanalysis* 26 (8), 1761–1772. doi:10.1002/elan.201400125

Roushani, M., Karami, E., Salimi, A., and Sahraei, R. (2013). Amperometric Detection of Hydrogen Peroxide at Nano-Ruthenium Oxide/riboflavin Nanocomposite-Modified Glassy Carbon Electrodes. *Electrochimica Acta* 113, 134–140. doi:10.1016/j.electacta.2013.09.069

Sajjadi Kouchesfehani, S. S., Keihan, A. H., Norouzi, P., Habibi, M. M., Eskandari, K., and Shirazi, N. H. (2017). Fabrication of an Amperometric Glucose Biosensor Based on a Prussian Blue/carbon Nanotube/ionic Liquid Modified Glassy Carbon Electrode. *J. Appl. Biotechnol. Rep.* 4 (2), 603–608.

Salimi, A., Rahmatpanah, R., Hallaj, R., and Roushani, M. (2013). Covalent Attachment of Thionine onto Gold Electrode Modified with Cadmium Sulfide Nanoparticles: Improvement of Electrocatalytic and Photelectrocatalytic Reduction of Hydrogen Peroxide. *Electrochimica Acta* 95, 60–70. doi:10.1016/j.electacta.2013.01.154

Shim, M., Shi Kam, N. W., Chen, R. J., Li, Y., and Dai, H. (2002). Functionalization of Carbon Nanotubes for Biocompatibility and Biomolecular Recognition. *Nano Lett.* 2 (4), 285–288. doi:10.1021/nl015692j

Shu, J., and Tang, D. (2020). Recent Advances in Photoelectrochemical Sensing: From Engineered Photoactive Materials to Sensing Devices and Detection Modes. *Anal. Chem.* 92 (1), 363–377. doi:10.1021/acs.analchem.9b04199

Sitnikova, N. A., Komkova, M. A., Khomyakova, I. V., Karyakina, E. E., and Karyakin, A. A. (2014). Transition Metal Hexacyanoferrates in Electrocatalysis of H2O2 Reduction: An Exclusive Property of Prussian Blue. *Anal. Chem.* 86 (9), 4131–4134. doi:10.1021/ac500595v

Solanki, P. R., Kaushik, A., Agrawal, V. V., and Malhotra, B. D. (2011). Nanostructured Metal Oxide-Based Biosensors. *NPG Asia Mater* 3 (1), 17–24. doi:10.1038/asiamat.2010.137

Srinivasan, B., Tung, S., and Tung, S. (2015). Development and Applications of Portable Biosensors. *J. Lab. Autom.* 20 (4), 365–389. doi:10.1177/2211068215581349

Stilwell, D. E., Park, K. H., and Miles, M. H. (1992). Electrochemical Studies of the Factors Influencing the Cycle Stability of Prussian Blue Films. *J. Appl. Electrochem* 22 (4), 325–331. doi:10.1007/bf01092684

Tang, H., Prasad, K., Sanjinès, R., Schmid, P. E., and Lévy, F. (1994). Electrical and Optical Properties of TiO2anatase Thin Films. *J. Appl. Phys.* 75 (4), 2042–2047. doi:10.1063/1.356306

Troitzsch, U., and Ellis, D. J. (2004). High-PT Study of Solid Solutions in the System ZrO2-TiO 2: The Stability of Srilankite. *ejm* 16 (4), 577–584. doi:10.1127/0935-1221/2004/0016-0577

Wan, Y., Ma, J., Zhou, W., Zhu, Y., Song, X., and Li, H. (2004). Preparation of Titania-Zirconia Composite Aerogel Material by Sol-Gel Combined with Supercritical Fluid Drying. *Appl. Catal. A Gen.* 277 (1–2), 55–59. doi:10.1016/j.apcata.2004.08.022

Wang, F.-T., Wang, Y.-H., Xu, J., Huang, K.-J., Liuhua, Z.-h., Lufei, Y.-f., et al. (2020). Boosting Performance of Self-Powered Biosensing Device with High-Energy Enzyme Biofuel Cells and Cruciform DNA. *Nano Energy* 68, 104310. doi:10.1016/j.nanoen.2019.104310

Wang, J. (2000). *Analytical*. Second Edition, 3. Wiley-V, 546–548.

Xu, J., Wang, Y.-H., Wei, Z., Wang, F.-T., and Huang, K.-J. (2021). Significantly Improving the Performance of Self-Powered Biosensor by Effectively Combining with High-Energy Enzyme Biofuel Cells, N-Doped Graphene, and Ultrathin Hollow Carbon Shell. *Sensors Actuators B Chem.* 327 (September 2020), 128933. doi:10.1016/j.snb.2020.128933

Yagi, Y., Briere, T. M., Sluiter, M. H. F., Kumar, V., Farajian, A. A., and Kawazoe, Y. (2004). Stable Geometries and Magnetic Properties of Single-Walled Carbon Nanotubes Doped with 3d Transition Metals: A First-Principles Study. *Phys. Rev. B - Condens Matter Mater Phys.* 69 (7), 1–9. doi:10.1103/physrevb.69.075414

Yan, Y., Miao, J., Yang, Z., Xiao, F.-X., Yang, H. B., Liu, B., et al. (2015). Carbon Nanotube Catalysts: Recent Advances in Synthesis, Characterization and Applications. *Chem. Soc. Rev.* 44 (10), 3295–3346. doi:10.1039/c4cs00492b

Yang, L., Zhang, H., Yu, S., Ding, Y., Cao, Y., Yang, F., et al. (2016). Carbon Supported CuPd Nanoparticles for Sensitive Detection and Electrocatalytic Reduction of M-Nitrophenol. *J. Electrochem. Soc.* 163 (6), B188–B191. doi:10.1149/2.0231606jes

Yang, S., Zhao, J., Tricard, S., Yu, L., and Fang, J. (2020). A Sensitive and Selective Electrochemical Sensor Based on N, P-Doped Molybdenum Carbide@Carbon/Prussian Blue/graphite Felt Composite Electrode for the Detection of Dopamine. *Anal. Chim. Acta* 1094, 80–89. doi:10.1016/j.aca.2019.09.077

Zhang, D., Wang, K., Sun, D. C., Xia, X. H., and Chen, H.-Y. (2003). Ultrathin Layers of Densely Packed Prussian Blue Nanoclusters Prepared from a Ferricyanide Solution. *Chem. Mat.* 15 (22), 4163–4165. doi:10.1021/cm034594r

Zhang, J., Lee, J.-K., Wu, Y., and Murray, R. W. (2003). Photoluminescence and Electronic Interaction of Anthracene Derivatives Adsorbed on Sidewalls of Single-Walled Carbon Nanotubes. *Nano Lett.* 3 (3), 403–407. doi:10.1021/nl025952c

Zhang, K., Lv, S., Zhou, Q., and Tang, D. (2020). CoOOH Nanosheets-Coated G-C3N4/CuInS2 Nanohybrids for Photoelectrochemical Biosensor of Carcinoembryonic Antigen Coupling Hybridization Chain Reaction with Etching Reaction. *Sensors Actuators B Chem.* 307 (December), 127631. doi:10.1016/j.snb.2019.127631

Zhang, M., Yuan, R., Chai, Y., Li, W., Zhong, H., and Wang, C. (2011). Glucose Biosensor Based on Titanium Dioxide-Multiwall Carbon Nanotubes-Chitosan Composite and Functionalized Gold Nanoparticles. *Bioprocess Biosyst. Eng.* 34 (9), 1143–1150. doi:10.1007/s00449-011-0565-4

Zhao, H., Liu, B., Li, Y., Li, B., Ma, H., and Komarneni, S. (2020). One-pot Green Hydrothermal Synthesis of Bio-Derived Nitrogen-Doped Carbon Sheets Embedded with Zirconia Nanoparticles for Electrochemical Sensing of Methyl Parathion. *Ceram. Int.* 46 (12), 19713–19722. doi:10.1016/j.ceramint.2020.04.277

Zong, S., Cao, Y., Zhou, Y., and Ju, H. (2007). Reagentless Biosensor for Hydrogen Peroxide Based on Immobilization of Protein in Zirconia Nanoparticles

Enhanced Grafted Collagen Matrix. *Biosens. Bioelectron.* 22 (8), 1776–1782. doi:10.1016/j.bios.2006.08.032

Zou, H., and Lin, Y. S. (2004). Structural and Surface Chemical Properties of Sol-Gel Derived TiO2-ZrO2 Oxides. *Appl. Catal. A General* 265 (1), 35–42. doi:10.1016/j.apcata.2004.01.015

Conflict of Interest: The authors declare that the research was conducted in the absence of any commercial or financial relationships that could be construed as a potential conflict of interest.

Publisher's Note: All claims expressed in this article are solely those of the authors and do not necessarily represent those of their affiliated organizations, or those of the publisher, the editors, and the reviewers. Any product that may be evaluated in this article, or claim that may be made by its manufacturer, is not guaranteed or endorsed by the publisher.